Octupole deformation in neutron-deficient plutonium isotopes

Hamid Ayatollahzadeh

IOP Conference University of Manchester
23.04.25 – 25.04.25

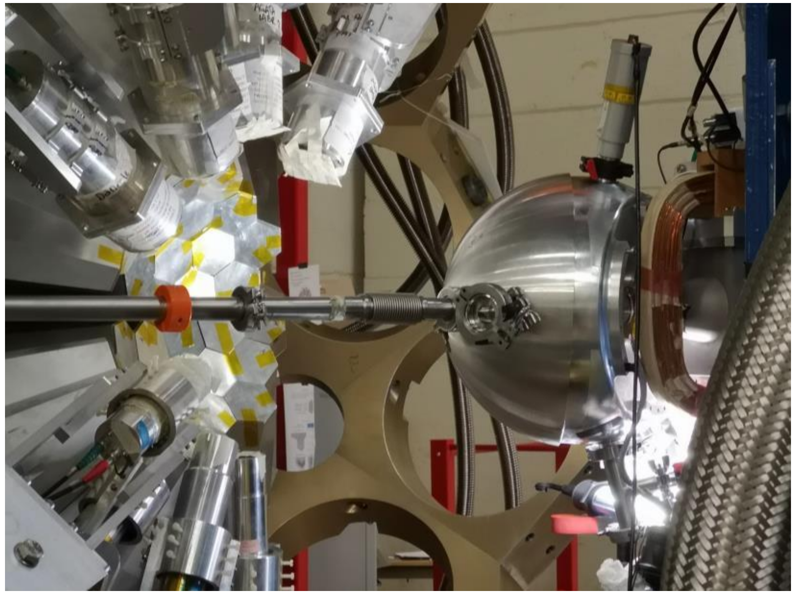

AGATA
ADVANCED GAMMA TRACKING ARRAY

INFN Istituto Nazionale di Fisica Nucleare
LABORATORI NAZIONALI DI LEGNARO

UWS UNIVERSITY OF THE WEST of SCOTLAND

Science & Technology Facilities Council

SUPA

Octupole deformation

The nuclear shape is described by spherical harmonics multiplied by an expansion coefficient (deformation parameter).

$$R(\theta, \phi) = R_0[1 + \sum_{\lambda,\mu} \alpha_{\lambda,\mu} Y_\lambda^\mu]$$

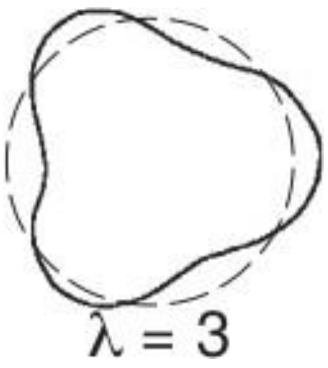

Spherical | Prolate | Oblate | Pear-shaped

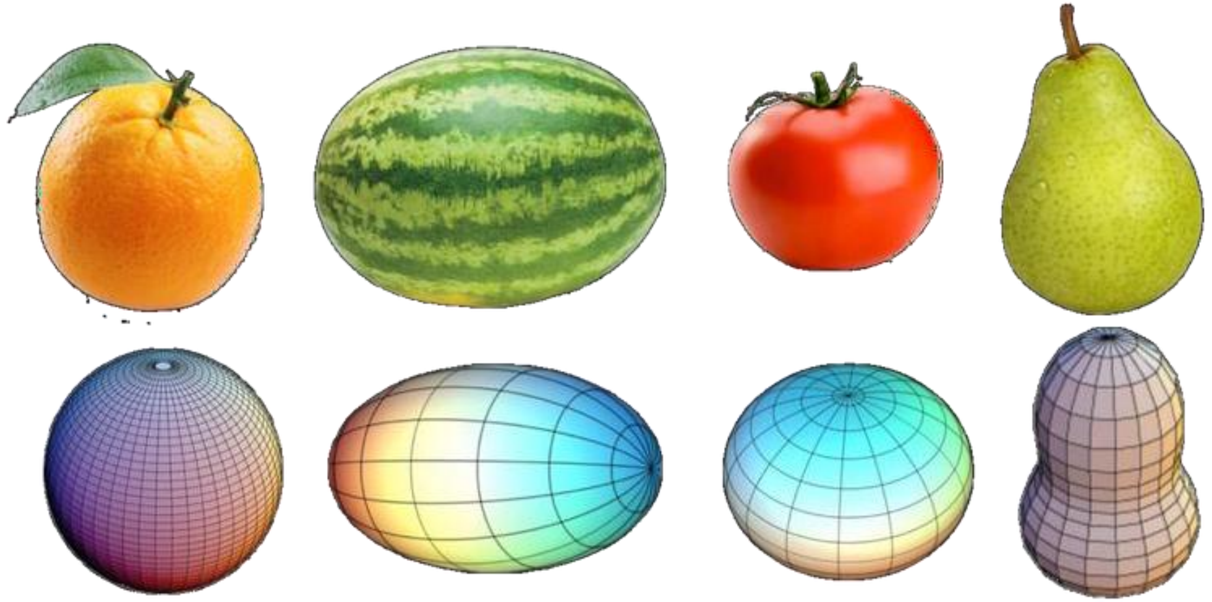

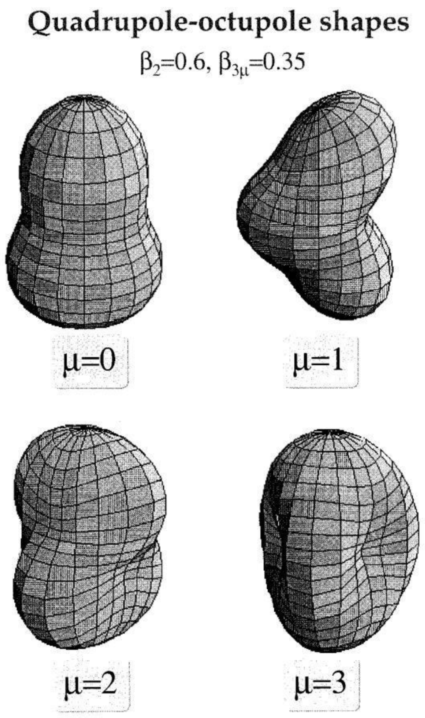

Octupole deformation

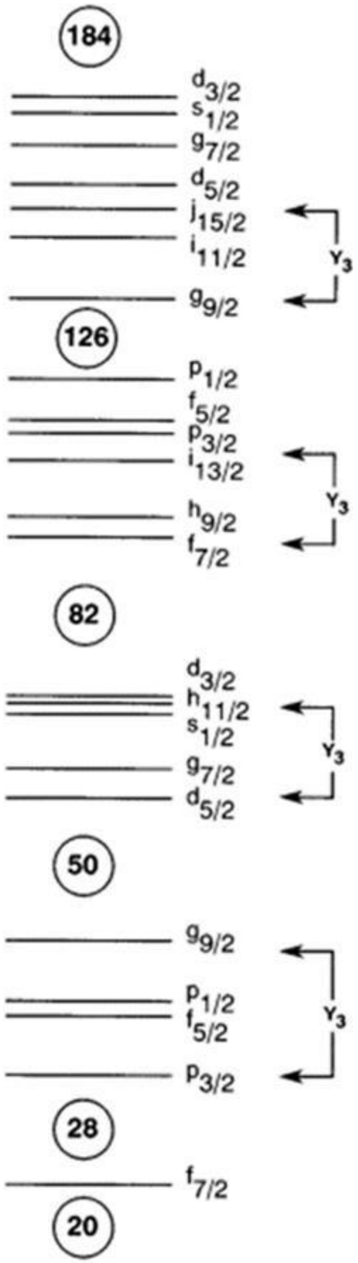

134 ($j_{15/2}$, $g_{9/2}$)

88 ($i_{13/2}$, $f_{7/2}$)

56 ($h_{11/2}$, $d_{5/2}$)

34 ($g_{9/2}$, $p_{3/2}$)

- $\Delta j = \Delta \ell = 3$
- Reflection-asymmetric nuclei
- Octupole magic numbers: 34, 56, 88, 134

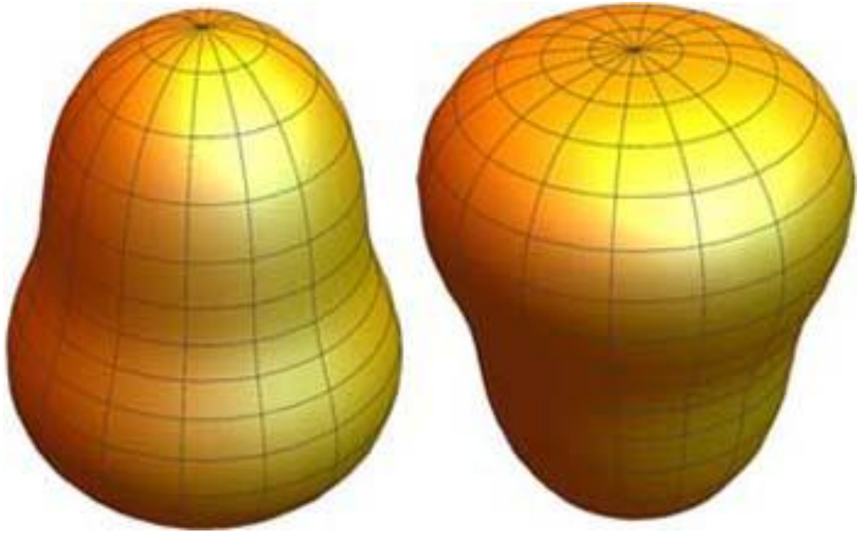

- N=Z=56 close to ^{112}Ba
- Z=56 N=88 close to ^{146}Ba
- Z=88 N=134 close to ^{224}Ra

Regional understanding

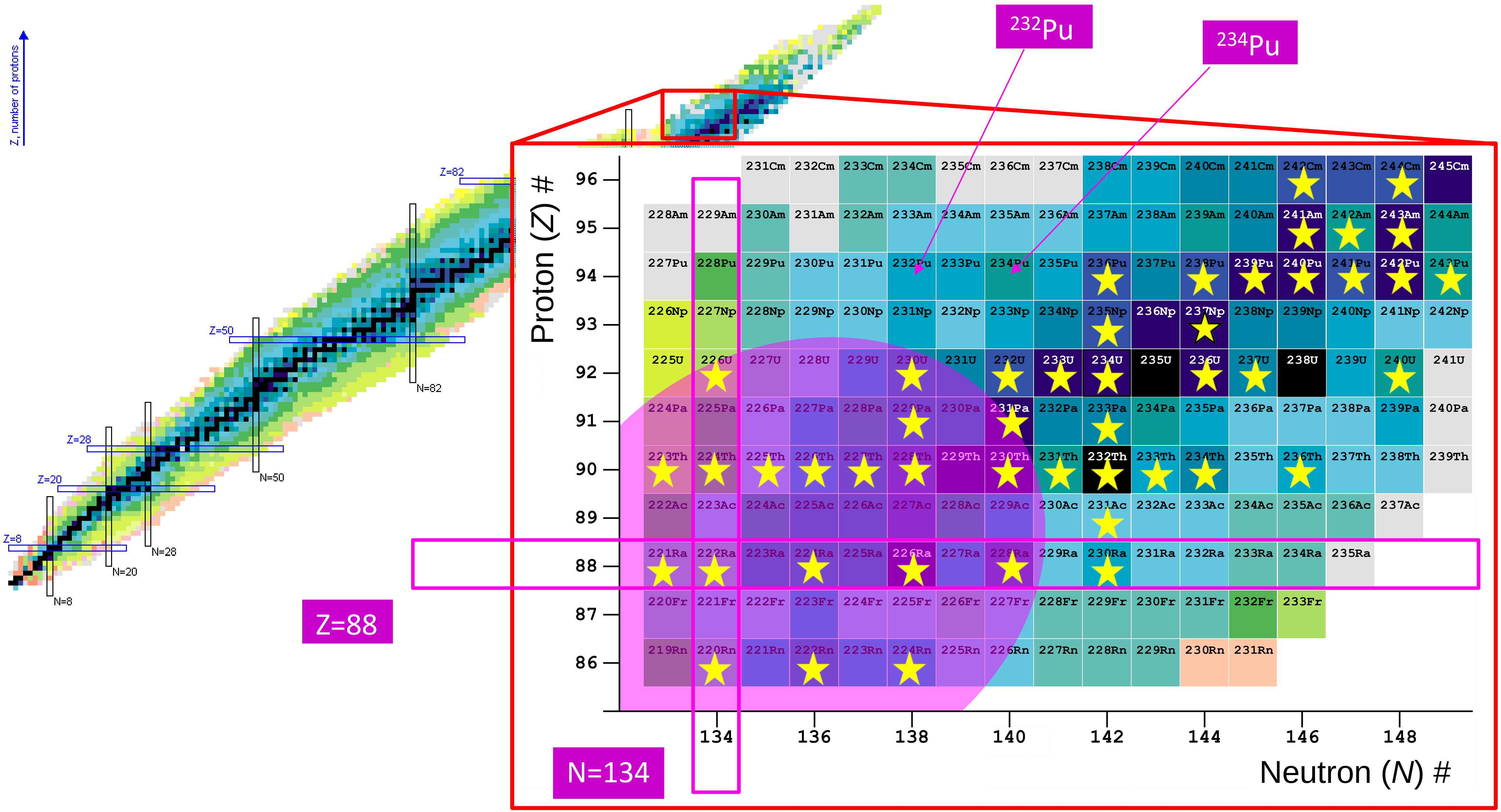

Previous plutonium studies

- An experiment by K. Abu Saleem et al. studied the ^{236}Pu isotope [K. Abu Saleem et al., Phys. Rev. C 70, 024310 (2004)] using the $^{237}Np(^{209}Bi,^{210}Pb)$ transfer reaction.
- Additional four γ-ray transitions identified in ^{236}Pu adding to established level scheme.

added γ rays

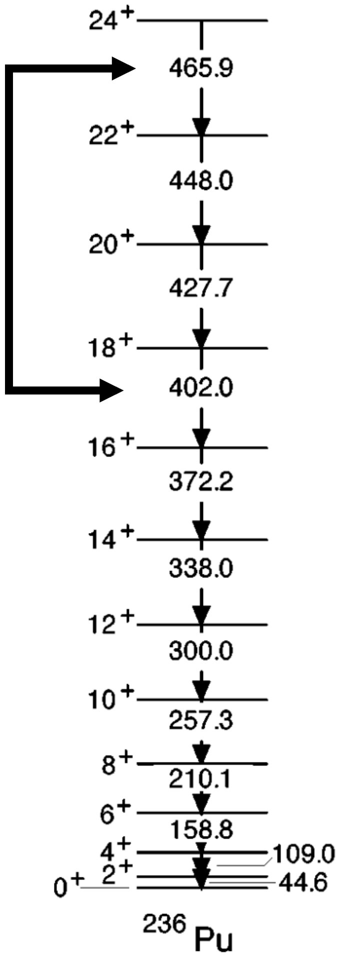

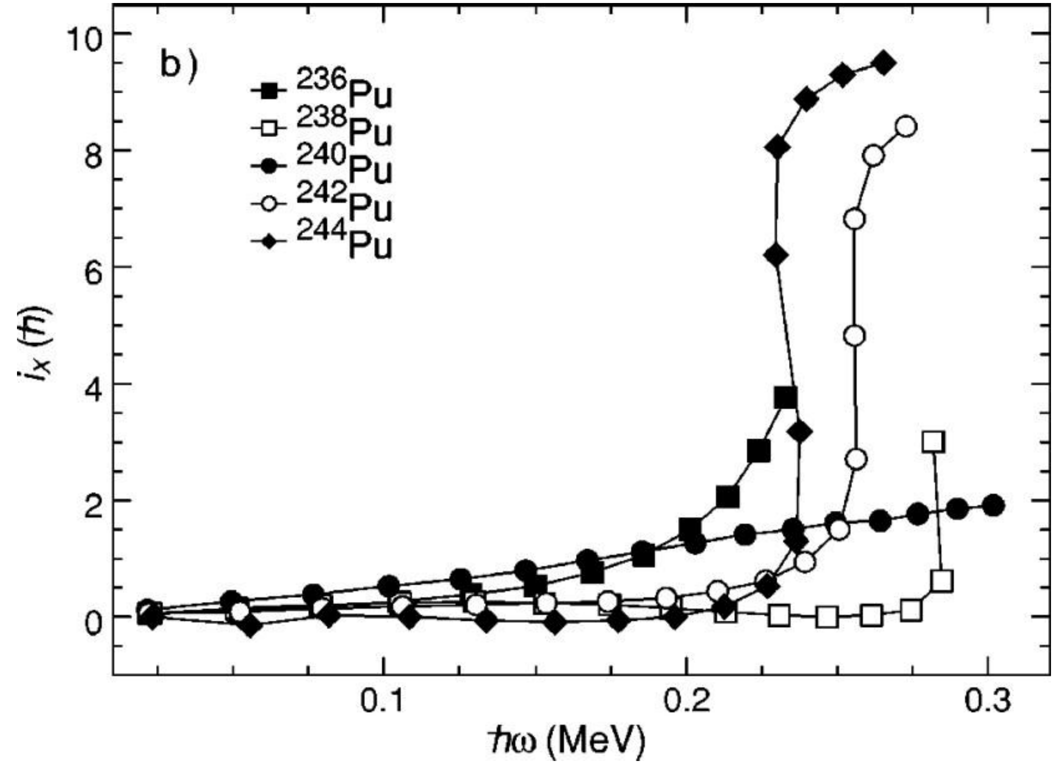

- Alignments show delayed backbending for plutonium isotopes with ^{236}Pu and ^{238}Pu.
- Only $^{238\text{-}240}Pu$ show interleaving alternating parity states indicating stronger octupole effects.

Theoretical predictions

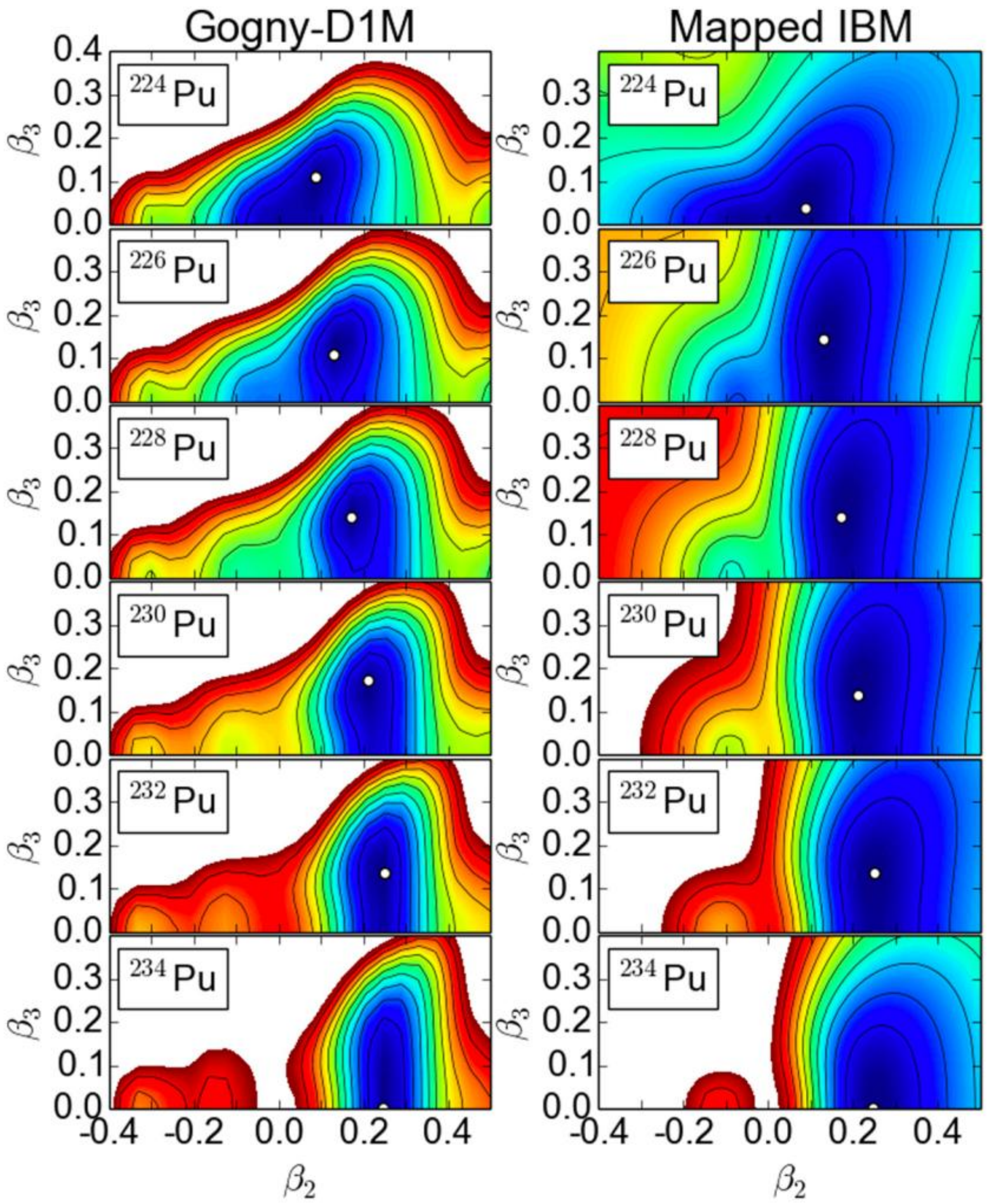

- Potential-energy surfaces measured by Nomura *et al.*
- ^{234}Pu has $\beta_3 \simeq 0$.
- ^{232}Pu has $\beta_3 \simeq 0.22$.

Multi-nucleon transfer reactions

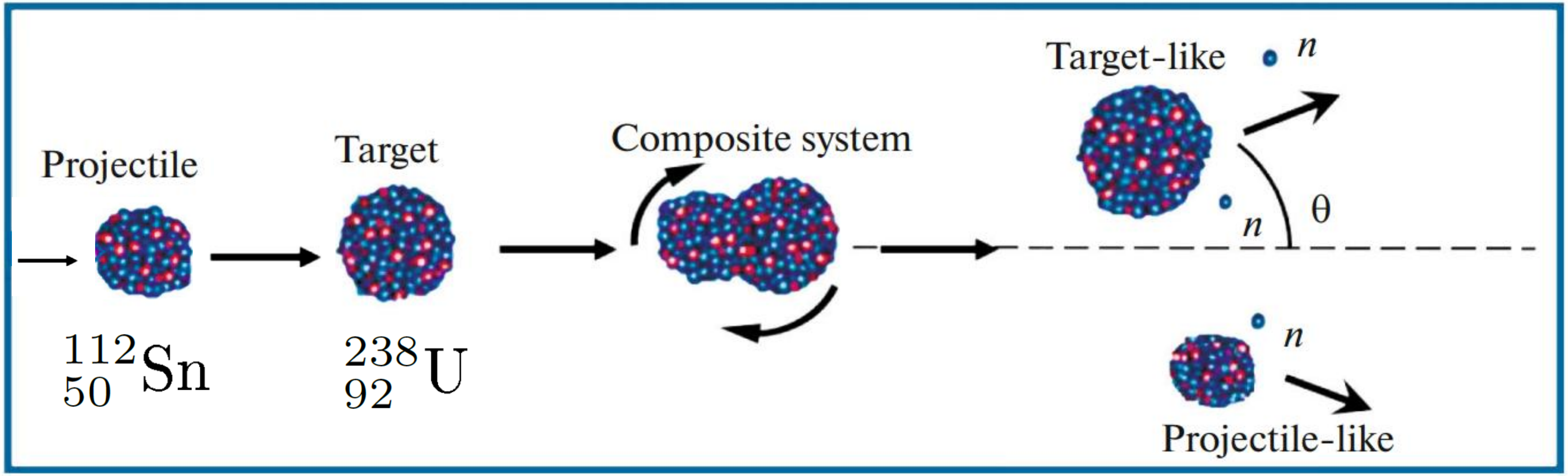

- Able to probe exotic nuclei past the current experimental limit when using fusion, fragmentation and other methods.
- Combination of MNT reactions with AGATA-PRISMA detector setup allows improved efficiency and selectivity.

Experimental details

$$^{112}_{50}\mathrm{Sn} + {}^{238}_{92}\mathrm{U}$$

808 MeV

$$\rightarrow \; ^{116}_{48}\mathrm{Cd} + {}^{234}_{94}\mathrm{Pu} \quad (\sigma \sim 0.7 \text{ mb})$$

$$\rightarrow \; ^{118}_{48}\mathrm{Cd} + {}^{232}_{94}\mathrm{Pu} \quad (\sigma \sim 0.4 \text{ mb})$$

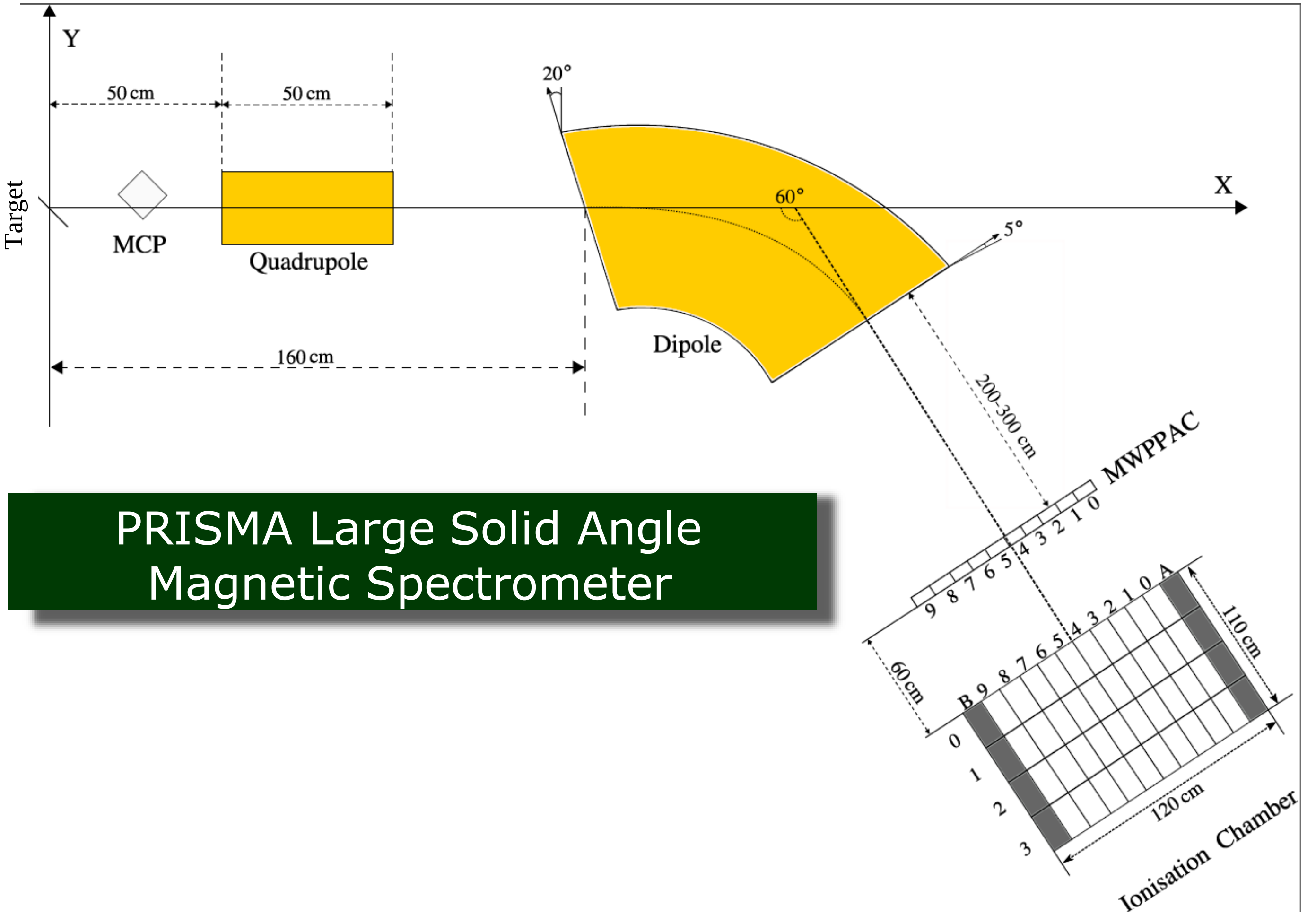

PRISMA Large Solid Angle Magnetic Spectrometer

AGATA
(Advanced GAmma Tracking Array)

AGATA- Advanced Gamma-ray Tracking Array

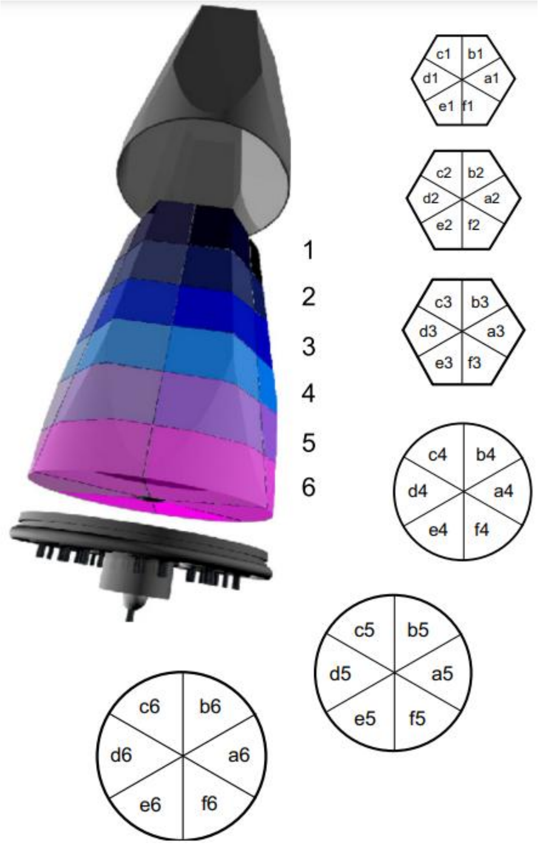

- New generation of gamma-ray spectrometers.
- Employs the novel technique of gamma-ray tracking to reconstruct events.
- 13 triple clusters.
- 36-fold segmentation.

AGATA - Gamma-ray tracking

- Segmented germanium crystals allows reconstruction of gamma-ray energy.
  - Two algorithms are employed to determine correct interaction sequence.
    - Negates the requirement for Compton suppression and improves the overall detection efficiency of the apparatus.

	Photopeak efficiency (%)	Peak/Total
Forward-tracking	53.6 (35.8)	75.2 (56.8)
Backtracking	36.7 (23.4)	67.4 (46.9)

- Multiplicity 1
- Multiplicity 30

Backtracking

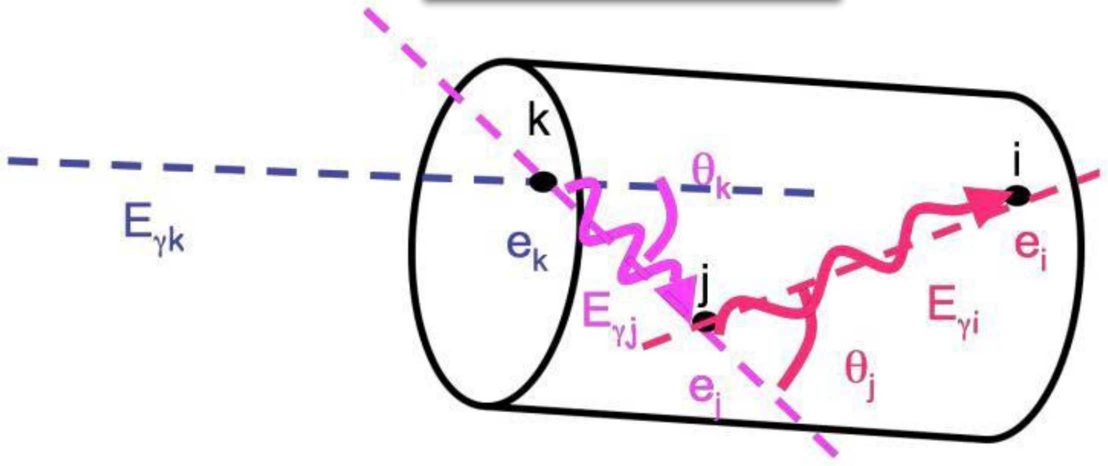

Forward Tracking

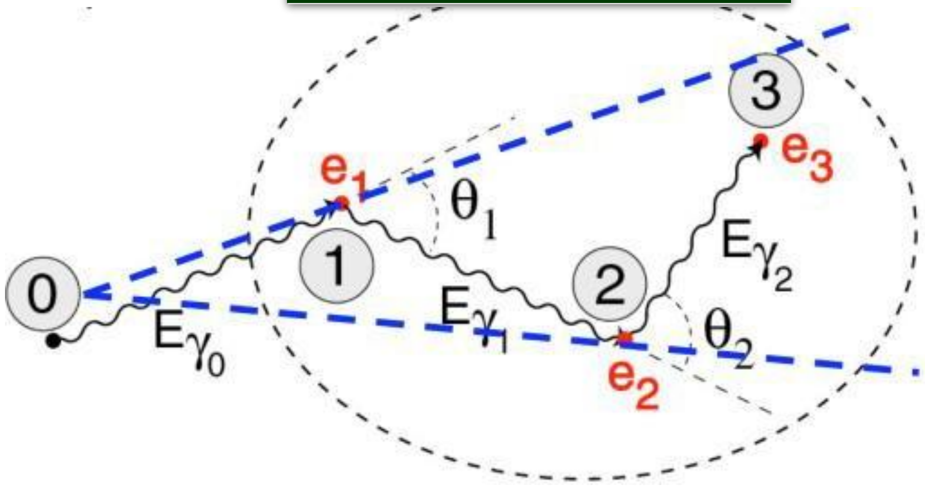

Experimental details

$$^{112}_{50}\mathrm{Sn} + {}^{238}_{92}\mathrm{U}$$

808 MeV

$$\rightarrow {}^{116}_{48}\mathrm{Cd} + {}^{234}_{94}\mathrm{Pu} \quad (\sigma \sim 0.7\ \mathrm{mb})$$

$$\rightarrow {}^{118}_{48}\mathrm{Cd} + {}^{232}_{94}\mathrm{Pu} \quad (\sigma \sim 0.4\ \mathrm{mb})$$

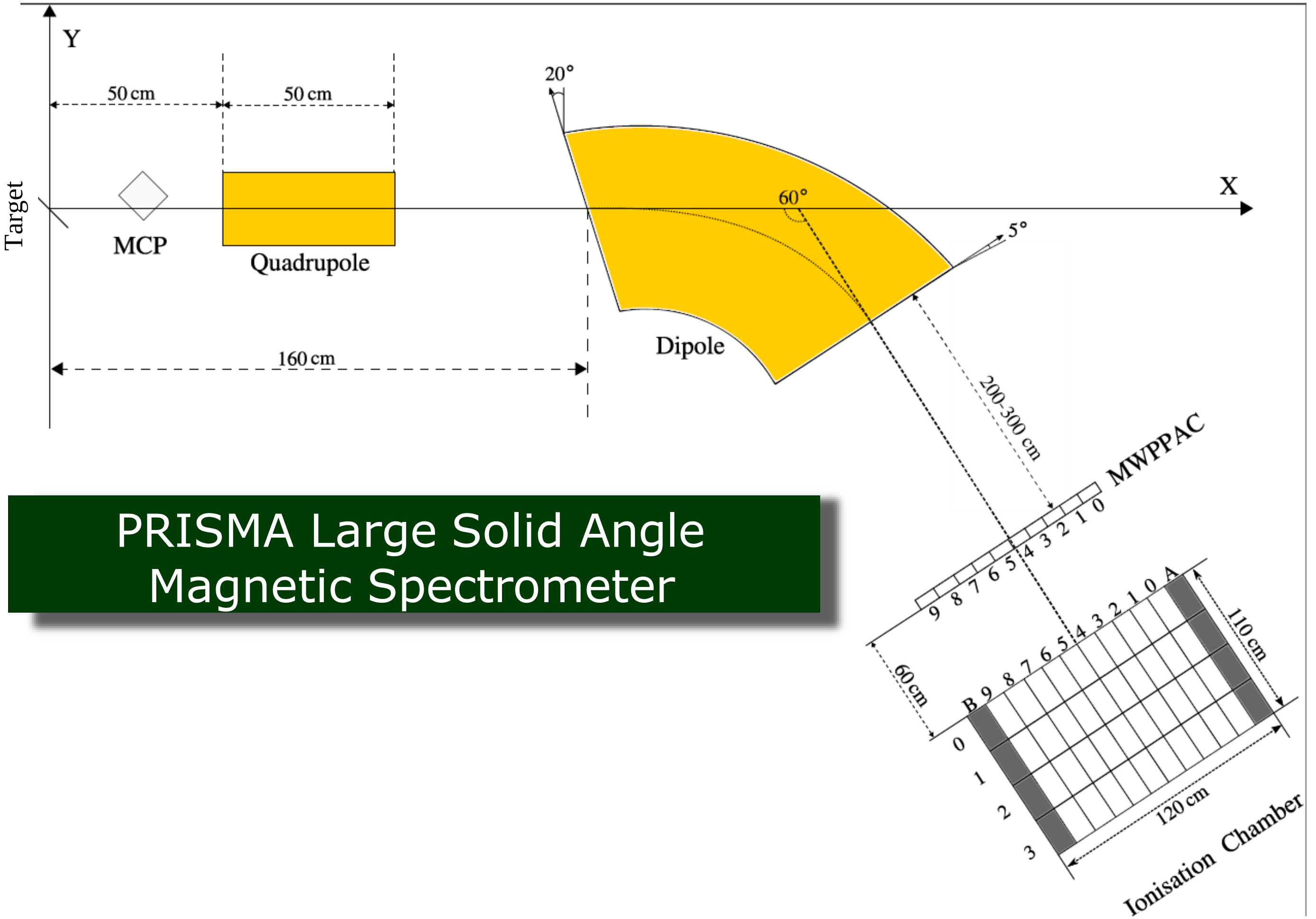

PRISMA Large Solid Angle Magnetic Spectrometer

AGATA
(Advanced GAmma Tracking Array)

PRISMA Magnetic Spectrometer

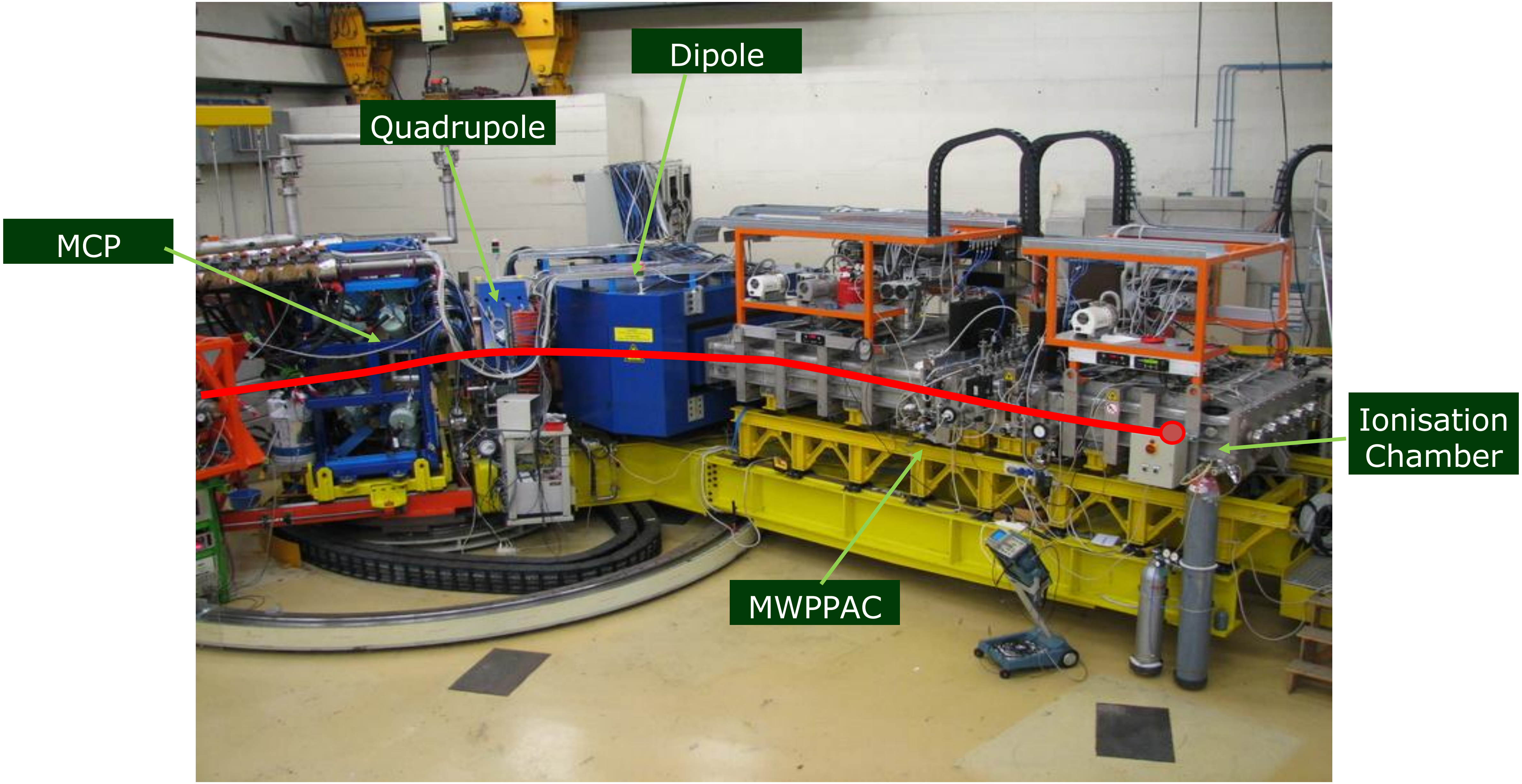

PRISMA - Analysis

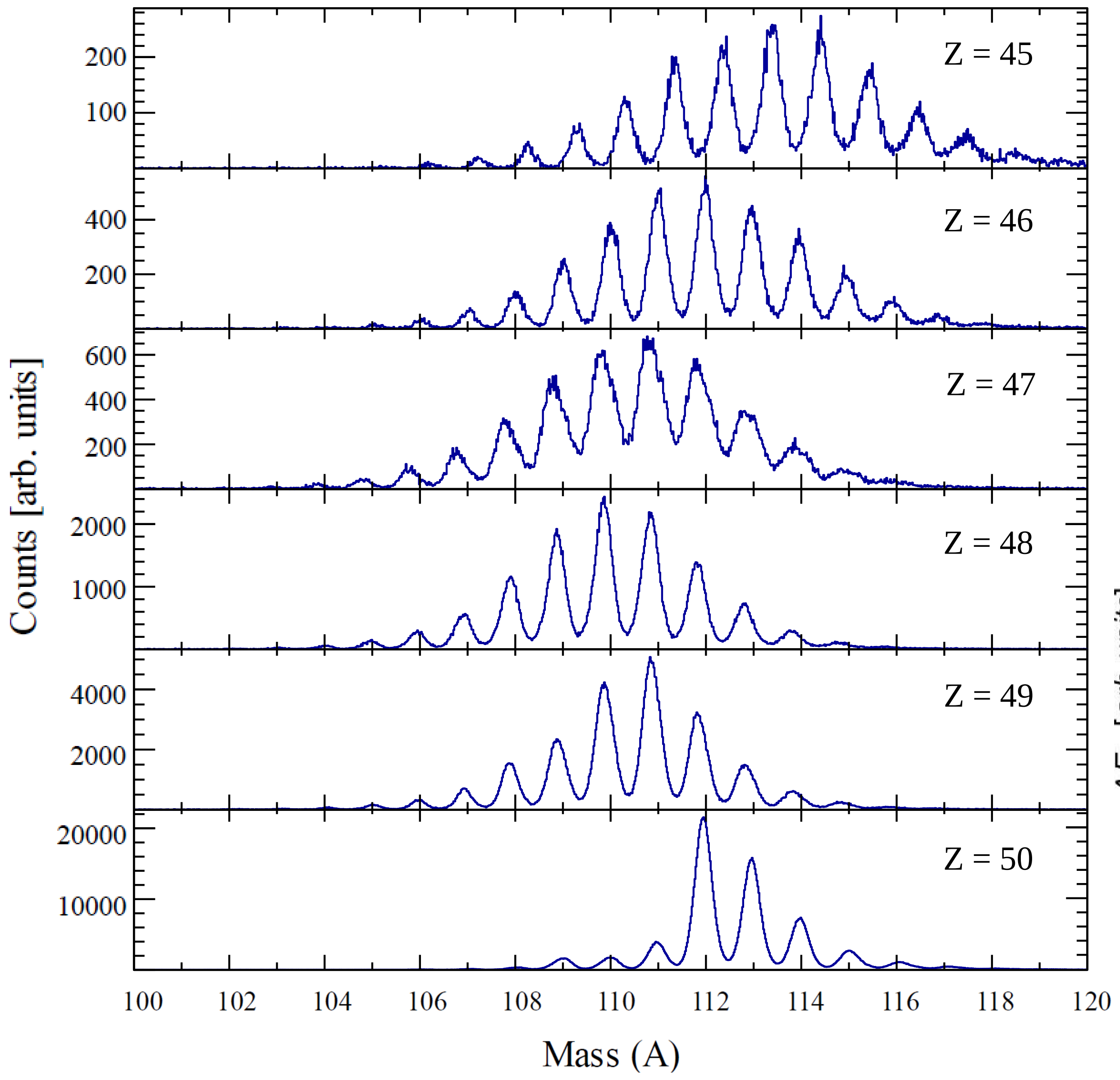

1. *Z* identification
2. *q* selection
3. Trajectory reconstruction
4. Aberrational corrections
4. *A*/*q* calibration
5. Mass calibration

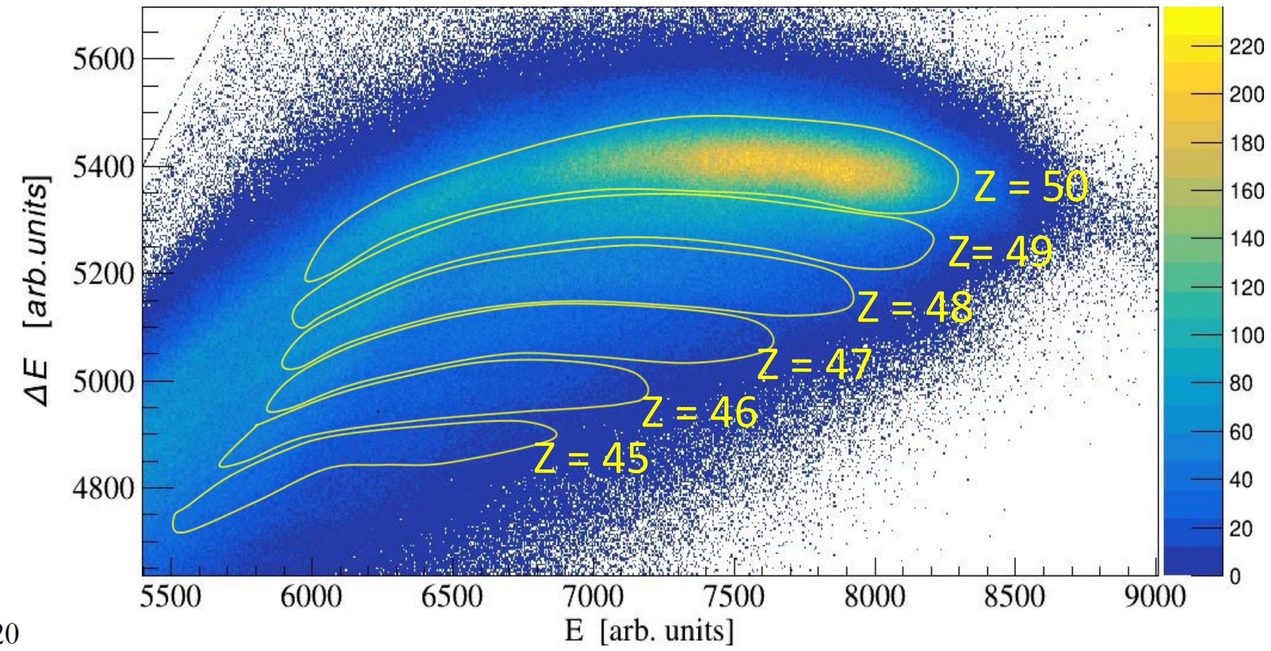

Analysis results – AGATA PRISMA coincidences

^{236}Pu Doppler corrected AGATA-PRISMA spectrum

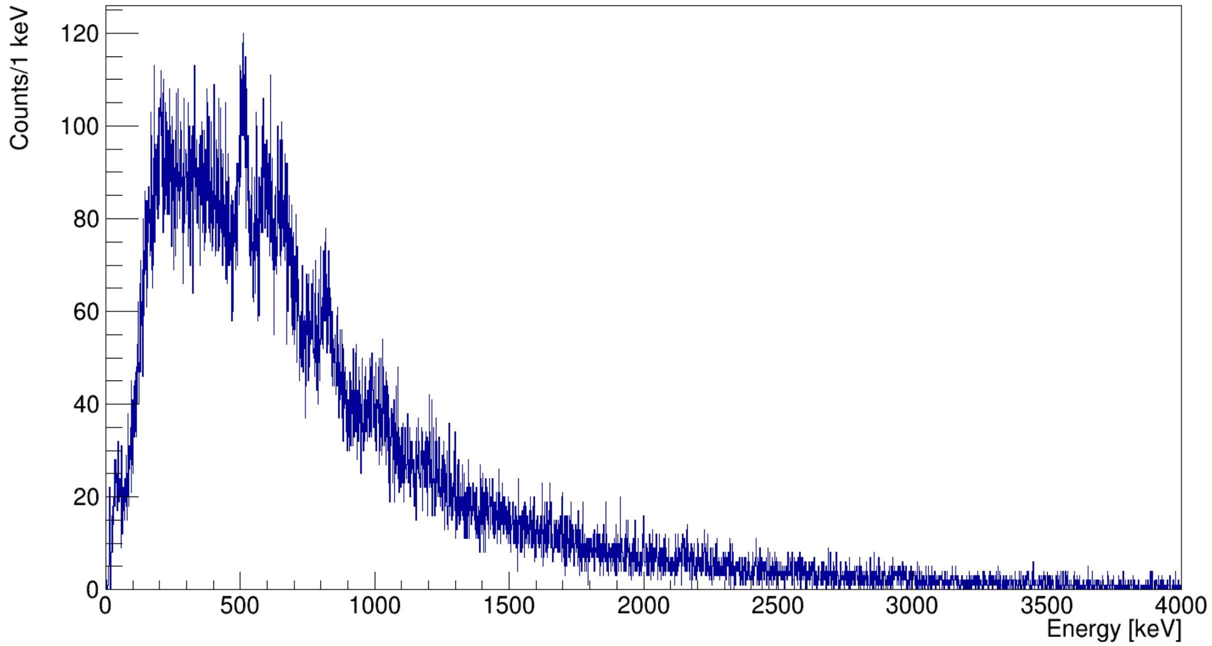

^{234}Pu Doppler corrected AGATA-PRISMA spectrum

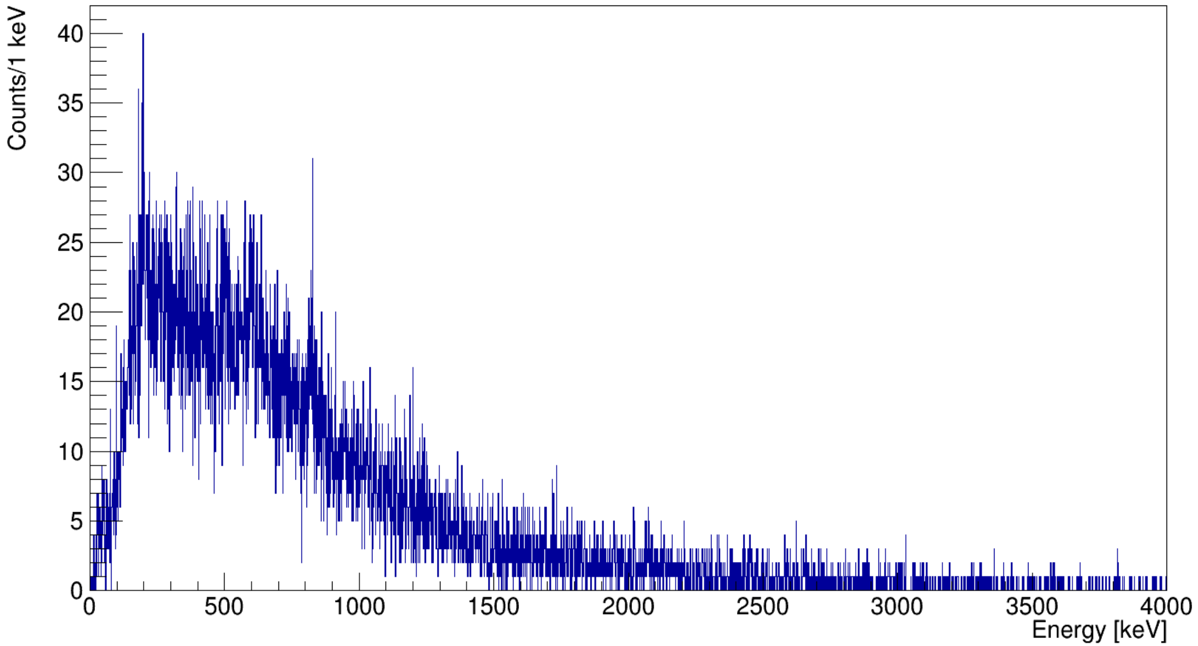

Analysis results – AGATA PRISMA coincidences

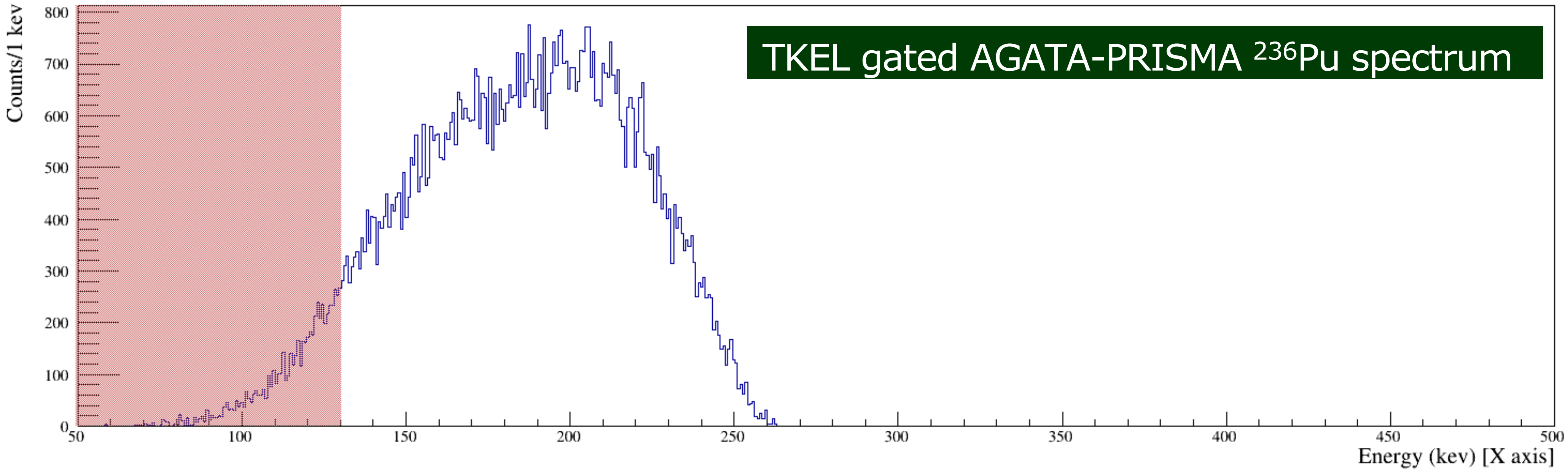

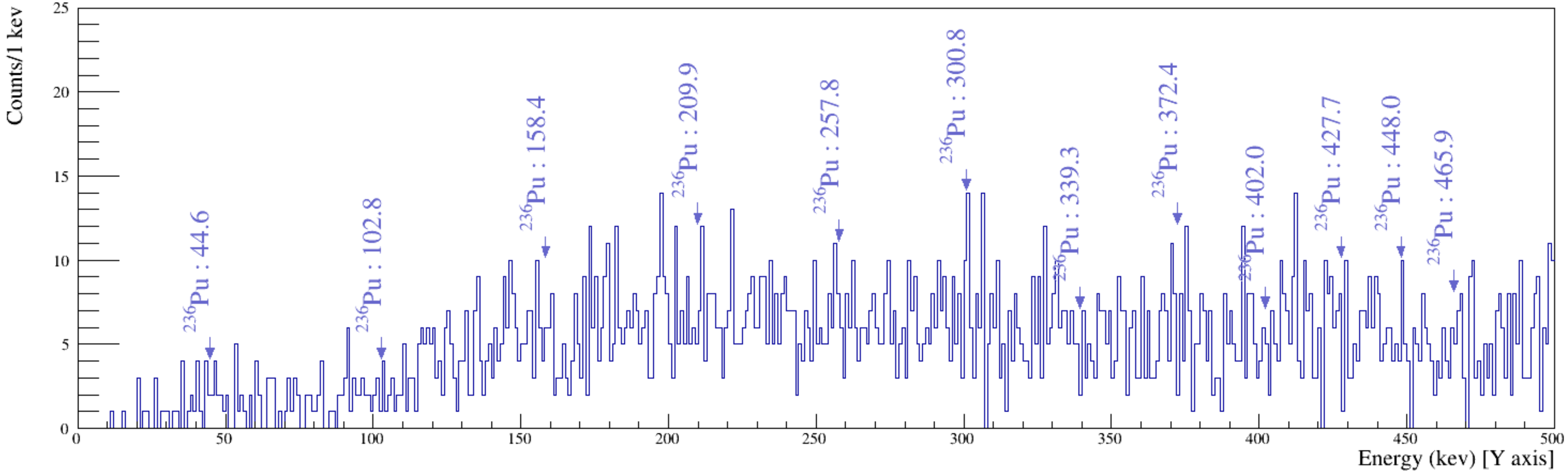

Analysis results – AGATA PRISMA coincidences

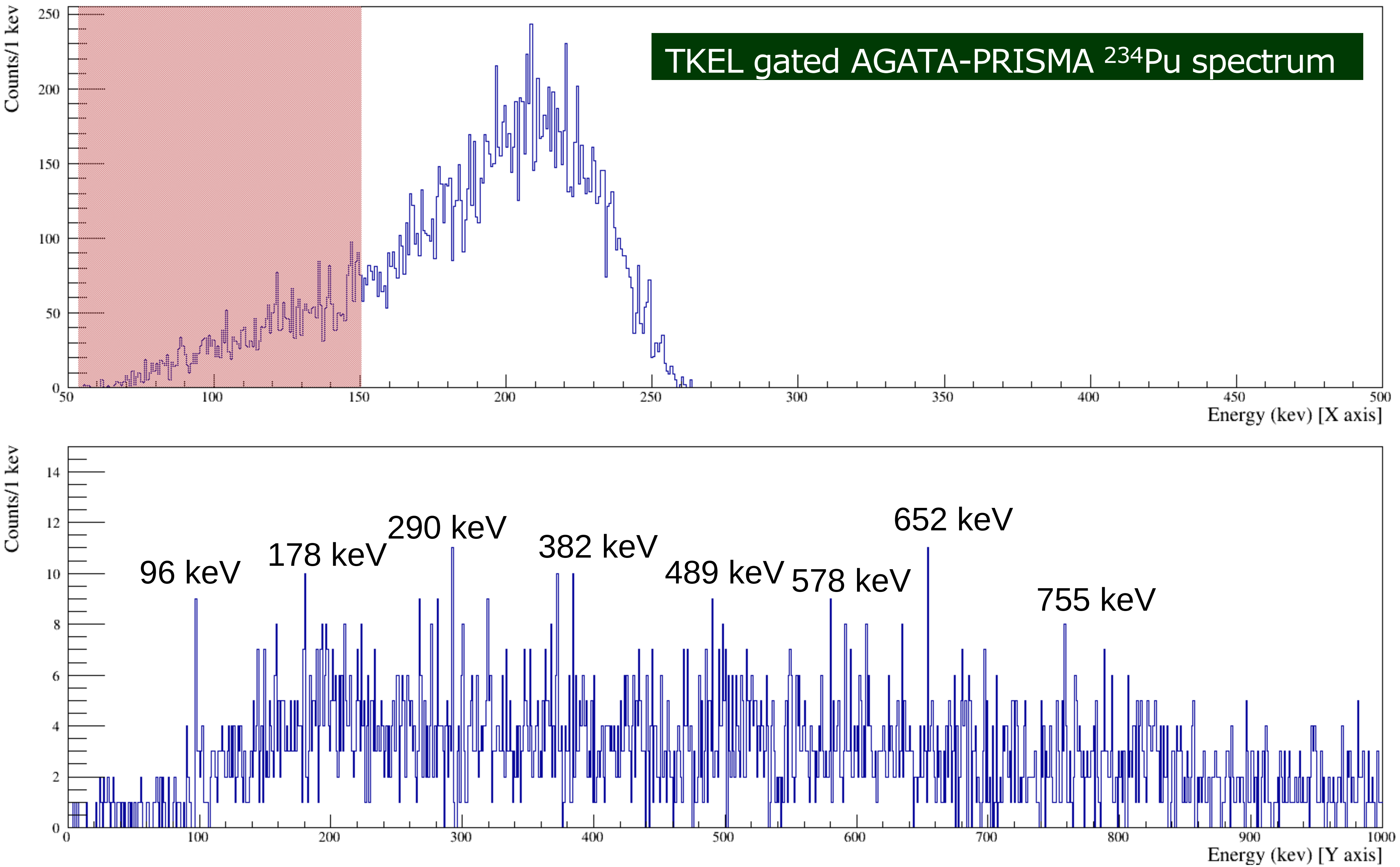

DANTE array

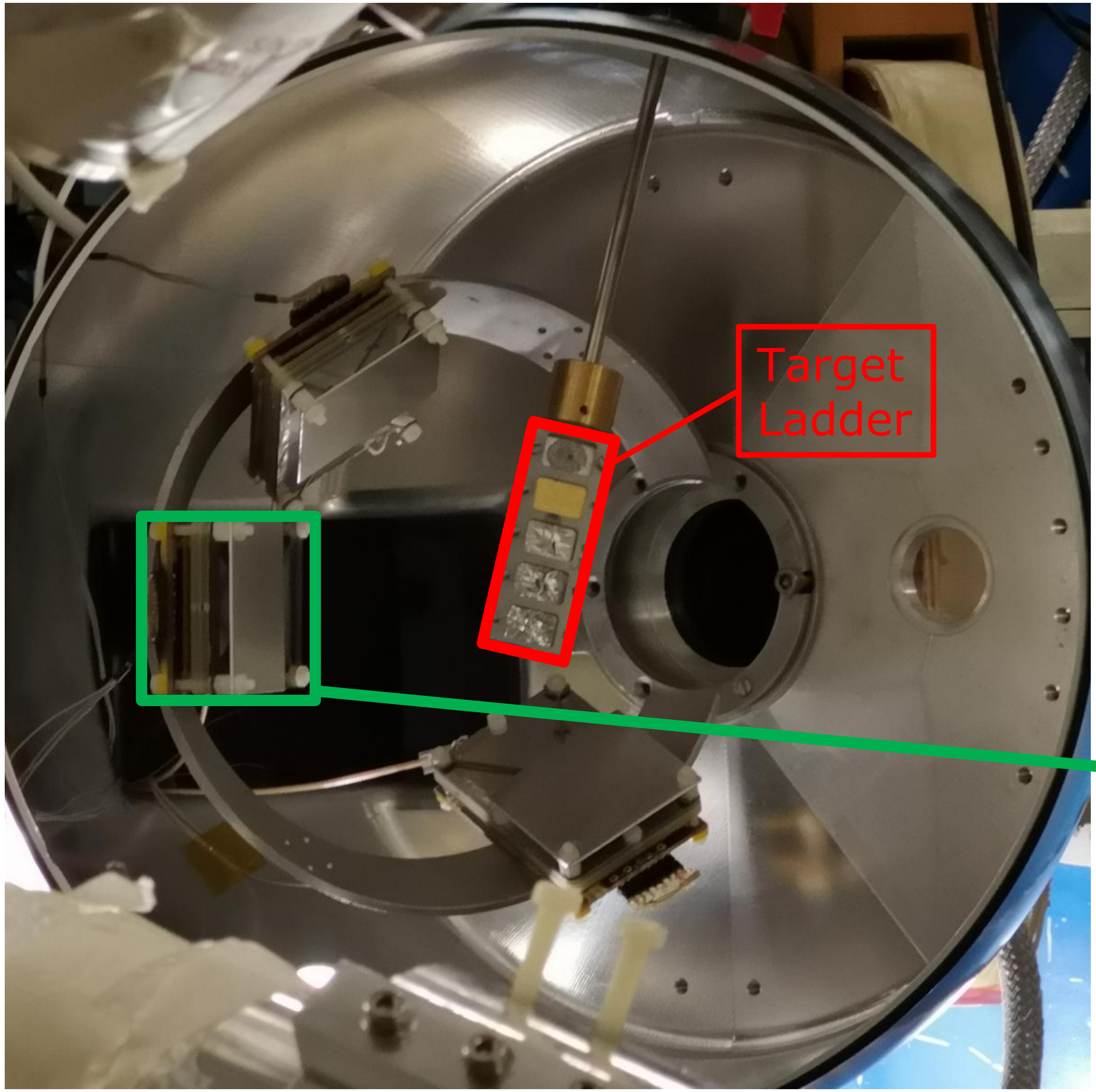

DANTE consisted of 3 detectors around the target position

Grazing angle of 56°

DANTE detector opposite PRISMA used for TOF measurements.

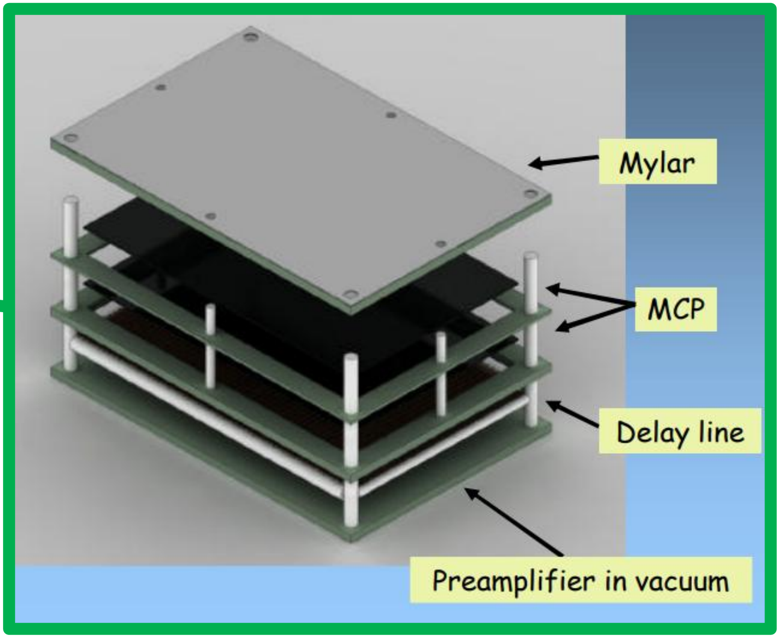

DANTE Analysis

1. Time alignment of DANTE with AGATA and PRISMA
2. Calibration of DANTE position (matrix)
3. Gate on TKEL - ΔTOF distribution
4. Observe AGATA-PRISMA-DANTE gated gammas.

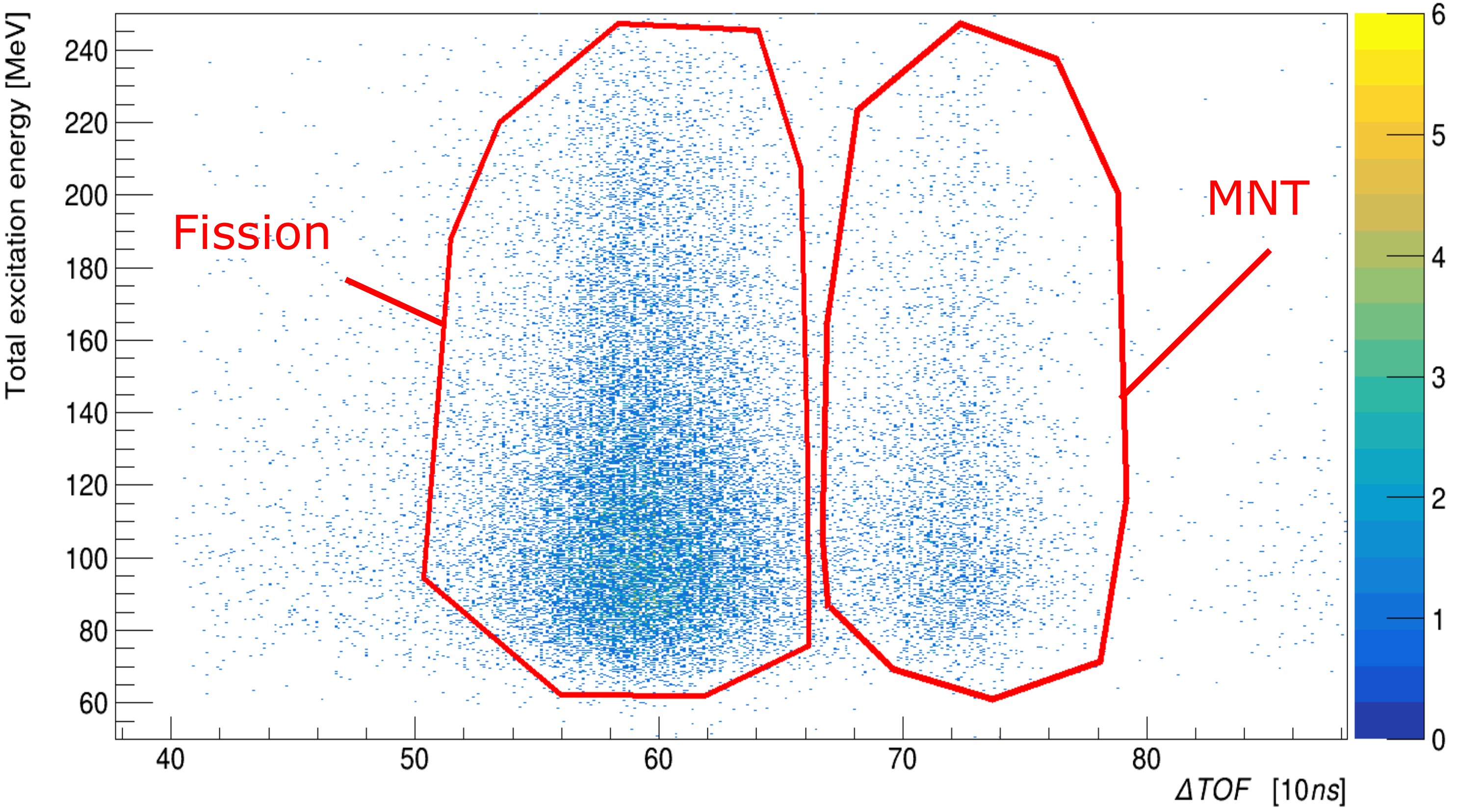

Analysis results – AGATA PRISMA DANTE coincidences

Doppler corrected ^{236}Pu gammas gated on TKEL - ΔTOF

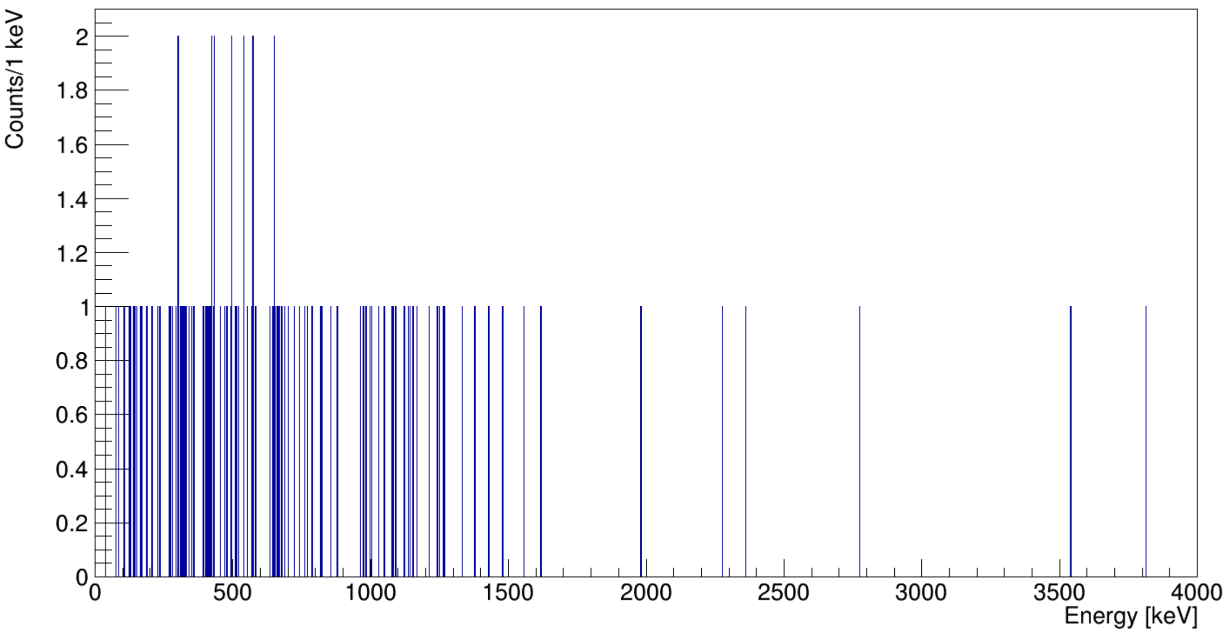

Doppler corrected ^{234}Pu gammas gated on TKEL - ΔTOF

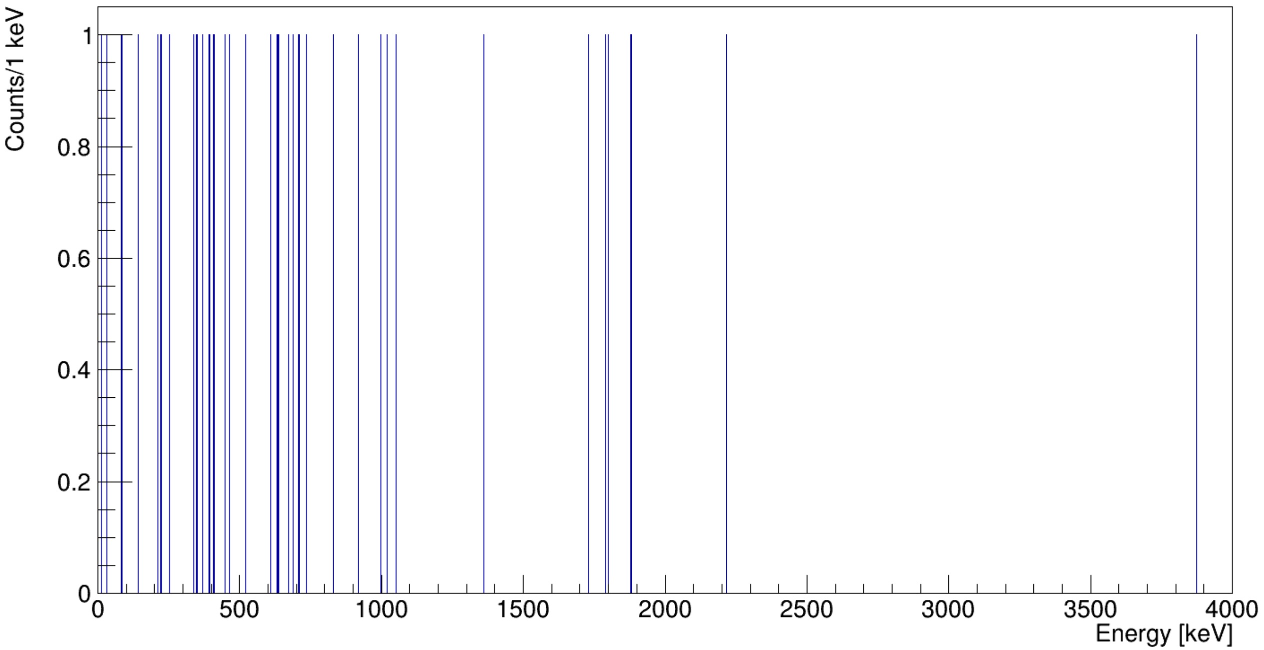

Next Steps

Conclusions:

- AGATA and PRISMA Analysis has been completed.
- Preliminary AGATA-PRISMA-DANTE results
- TKEL gating shows another method of selectivity.

Next steps:

- Confirm DANTE statistics are as shown.
- Conduct TKEL gating in more detail on Pu nuclei.
- Look at projectile-like reaction products In, Ag, Pd for new transitions.

Summary

With thanks to all collaborators:

H. Ayatollahzadeh [1, 2], J. M. Keatings [1, 2], J. F. Smith [1, 2], D. Mengoni [3], P. Aguilera [3, 4], G. Andreetta [3, 5], F. Angelini [3, 4], M. Balogh [4], J. Benito [3, 4], M. A. Bentley [6], A. J. Boston [7], H. C. Boston [7], S. Bottoni [8, 9], M. Bowry [1, 2], P. A. Butler [7], D. Brugnara [4], S. Carollo [3], G. Corbari [8], L. Corradi [4], R. Escudeiro [5], P. T. Greenlees [10], R. Chapman [1, 2], D. M. Cullen [1, 2,] G. de Angelis [4], A. Ertoprak [4], C. Everett [7], L. P. Gaffney [7], F. Galtarossa [5], A. Goasduff [4], B. Góngora Servín [4, 11], A. Gottardo [4], A. Gozzelino [4], J. Hackett [7], S. D. Hart [12], F. Holloway [7], P. M. Jones [12], S. Jongile [12], D. Judson [7], M. Labiche [13], M. S. R. Laskar [9], K. L. Malatji [12], A. McCarter [7], G. Montagnoli [3], N. Marchini [14], B. S. Nara Singh [1, 2], D. R. Napoli [4], R. Nicolás del Álamo [3, 5], D. O'Donnell [1, 2], J. Pellumaj [4], R. Pérez [4], S. Pigliapoco [3], E. Pilotto [5], M. Polettini [3], F. Recchia [3], K. Rezynkina [4], E. Rintoul [7], M. Rocchini [14], M. Sedlak [4], M. Siciliano [15], A. Stefanini [4], D. Stramaccioni [3, 4], C. Sullivan [7], J. J. Valliente-Dobon [4], F. van Niekerk [12], L. Zago [3, 4], and I. Zanon [4].

[1]School of Computing, Engineering, and Physical Sciences, University of the West of Scotland, Paisley, PA 1 2BE, United Kingdom
[2]Scottish Universities Physics Alliance (SUPA)
[3]Dipartimento di Fisica e Astronomia dell'Universitá di Padova, I-35131 Padova, Italy
[4]INFN, Laboratori Nazionalidi Legnaro, I-35020 Legnaro, Padova, Italy
[5]Istituto Nazionale di Fisica Nucleare, Sezionedi Padova, I-35131 Padova, Italy
[6]School of Physics, Engineering and Technology, University of York, Heslington, York YO10 5DD, United Kingdom
[7]Oliver Lodge Laboratory, University of Liverpool, Liverpool, L697ZE, United Kingdom
[8]Dipartimento di Fisica, Universitá degli Studi di Milano, 20133 Milano, Italy
[9]INFN Sezione di Milano, 20133, Milano, Italy
[10]University of Jyvaskyla, Department of Physics, P.O. Box 35, FIN-40014 University of Jyvaskyla, Finland
[11]Dipartimento di Fisicae Scienze della Terra, Università di Ferrara, Ferrara, Italy
[12]iThemba LABS, National Research Foundation, PO Box 722, Somerset West 7129, South Africa
[13]STFC Daresbury Laboratory, Daresbury, Warrington WA44AD, United Kingdom
[14]INFN Sezione di Firenze, IT-50019 Firenze, Italy
[15]Physics Division, Argonne National Laboratory, Argonne, USA

Spectroscopic features of octupole deformation

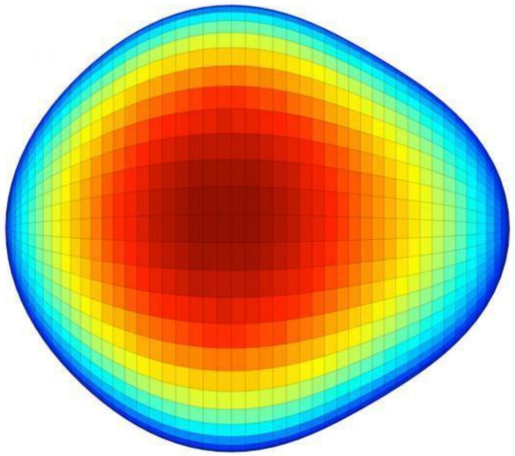

^{224}Ra

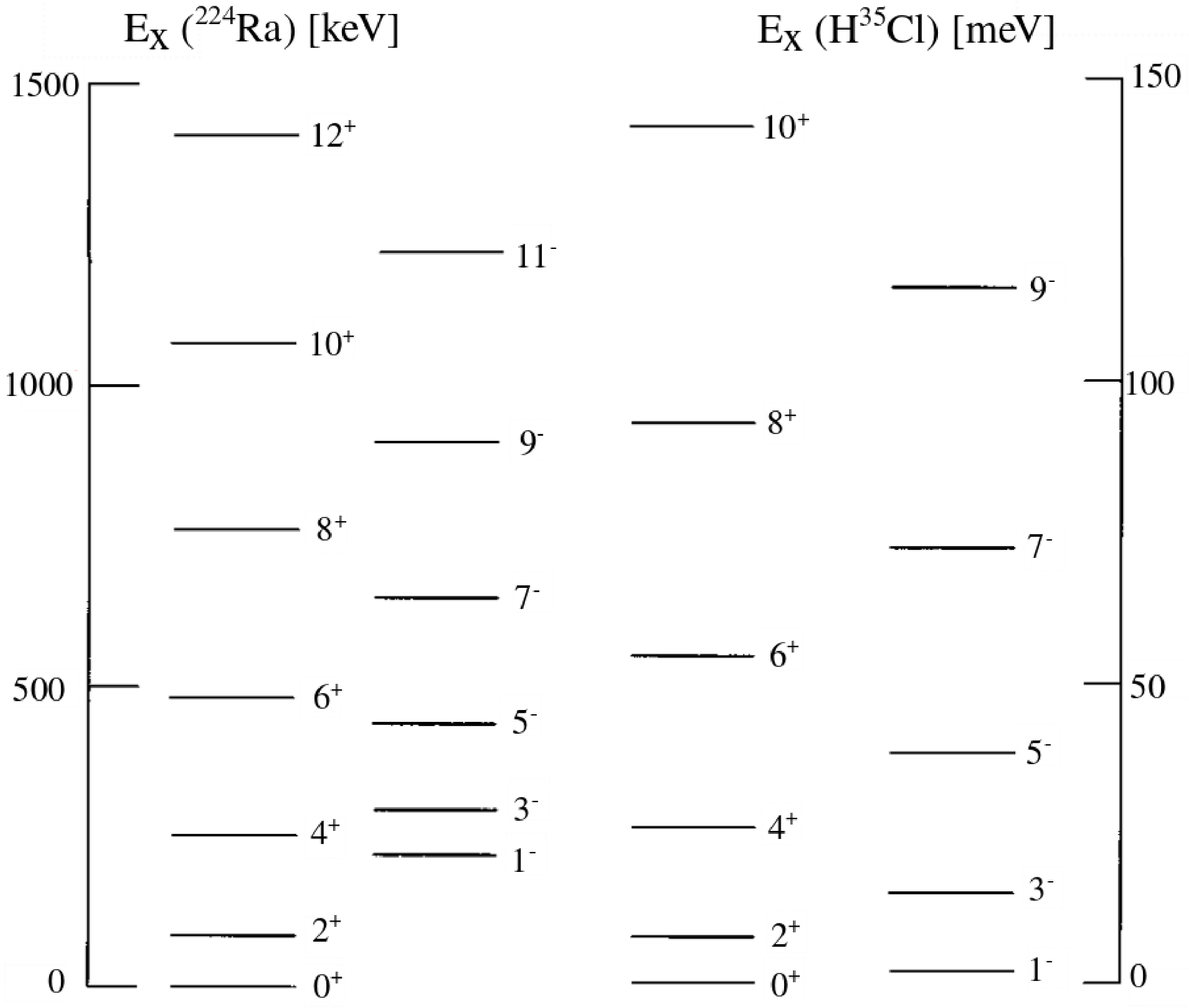

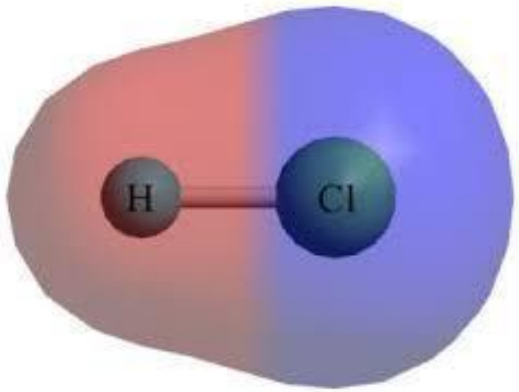

HCl

Spectroscopic features of octupole deformation

Angular momentum increasing

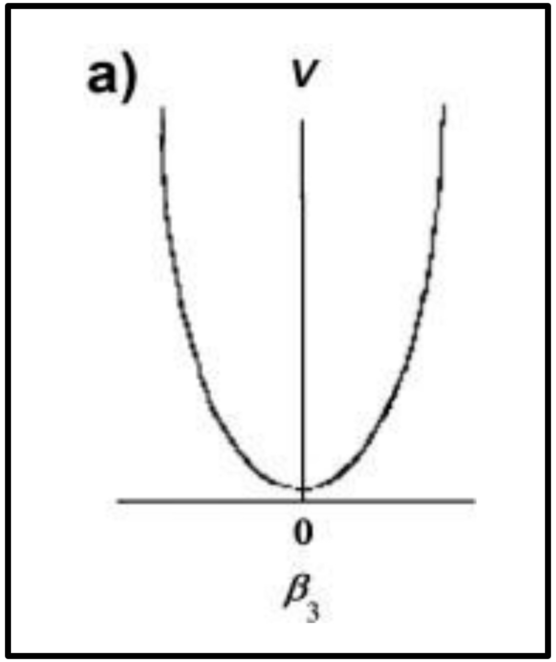

Octupole vibrational

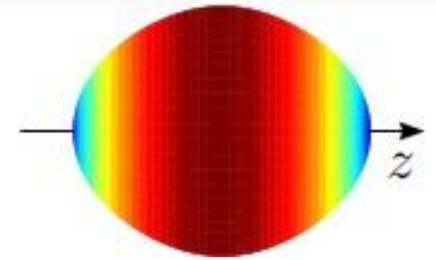

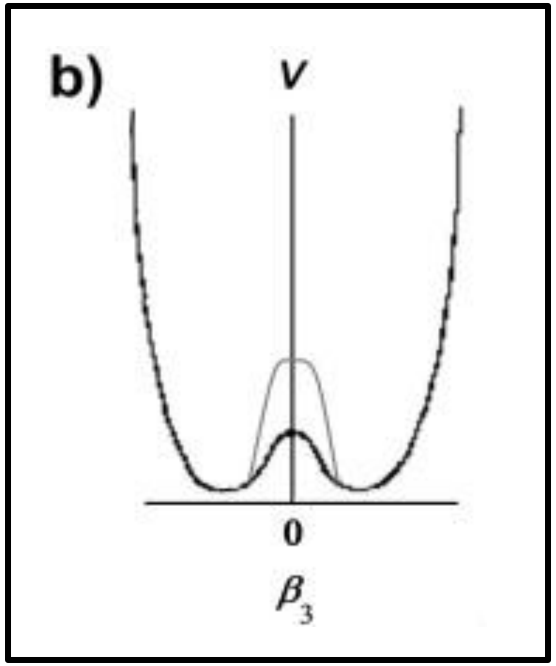

Octupole deformed (static)

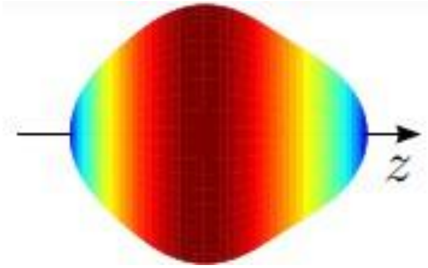

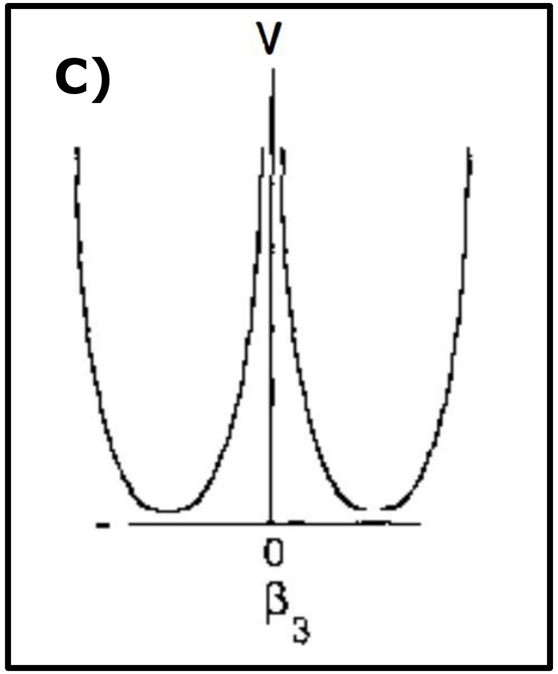

Octupole deformed (rigid)

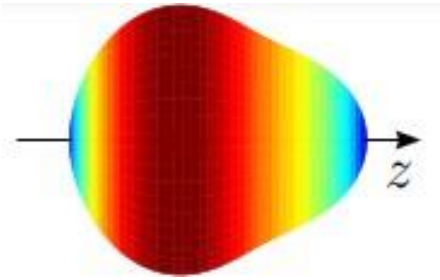

PRISMA - q selection

$$B\rho = \frac{p}{q}$$

$$p = mv\,,\quad E_k = \frac{1}{2}mv^2,\quad v = \beta c$$

$$E_k \propto q \cdot \rho\beta$$

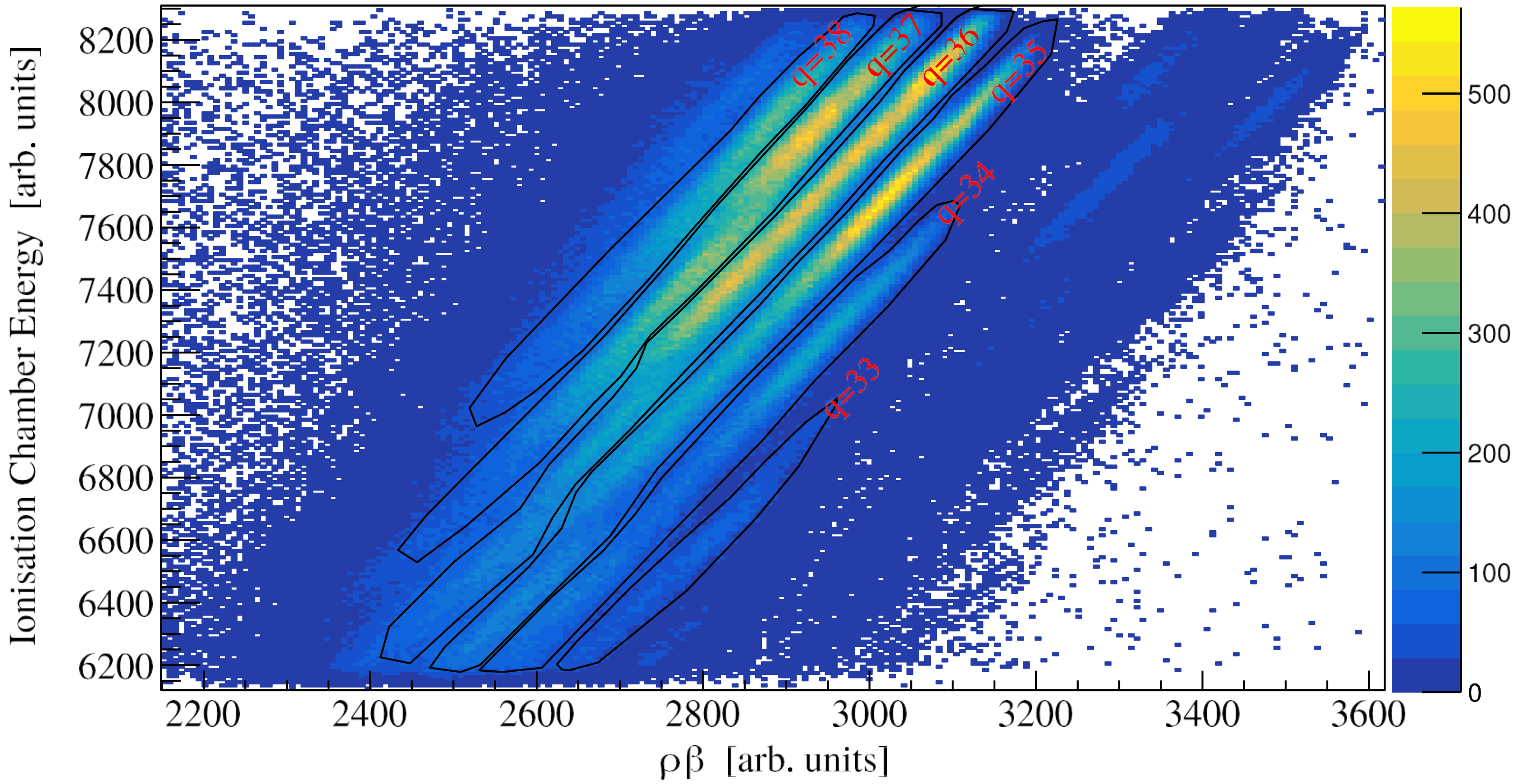

Charge state (q) gates applied to each Z gated distribution

PRISMA – Trajectory reconstruction

Bad optical parameters

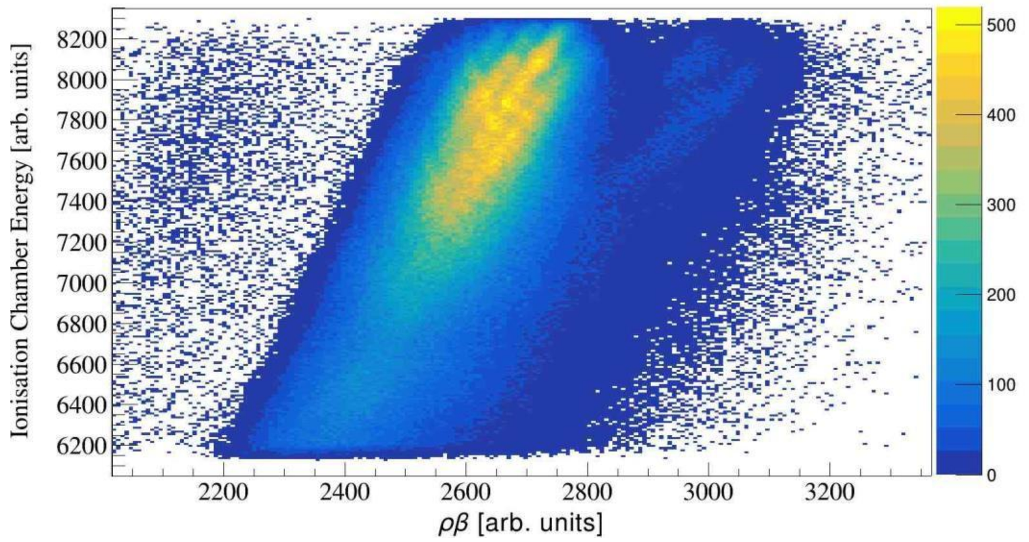

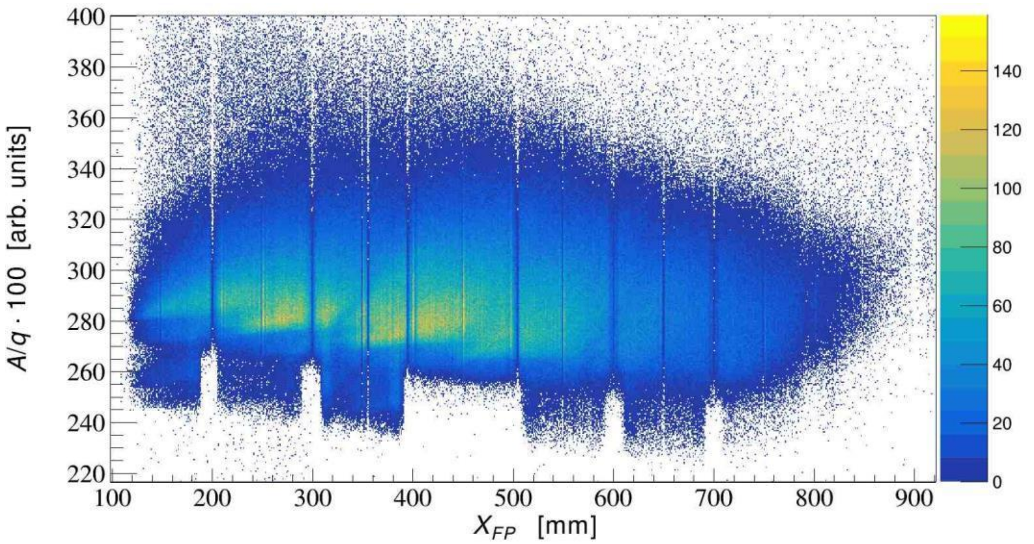

Good optical parameters

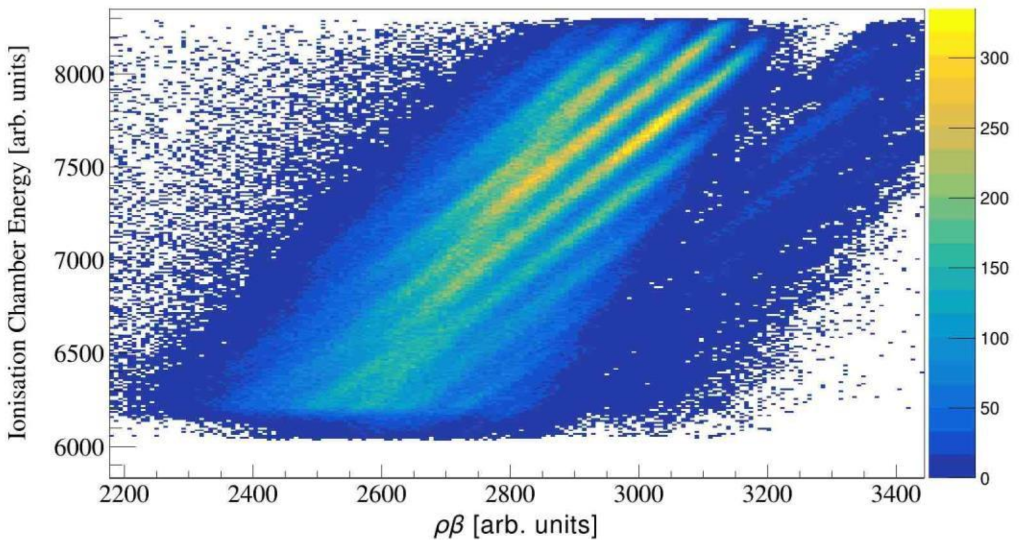

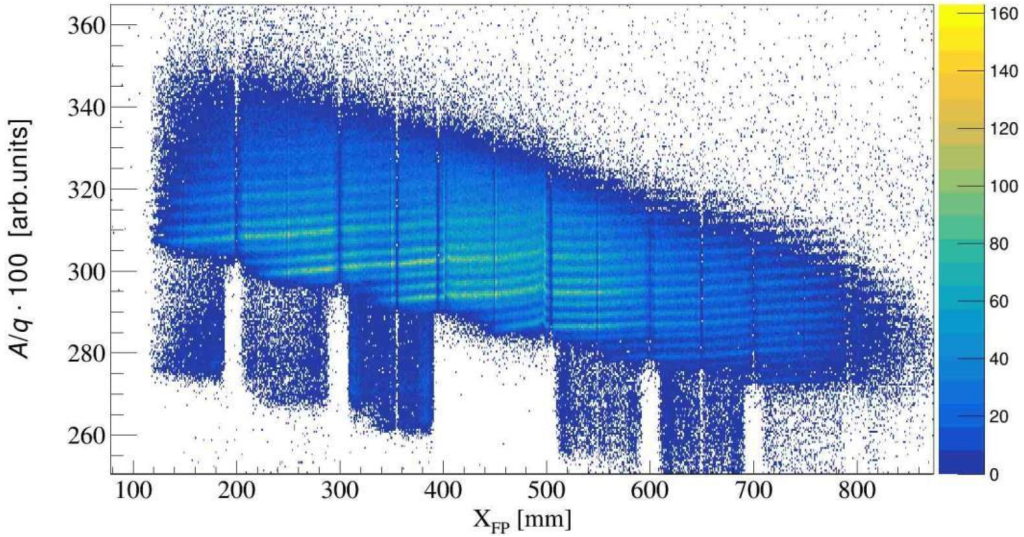

PRISMA - A/q calibration

Before Aberrational corrections

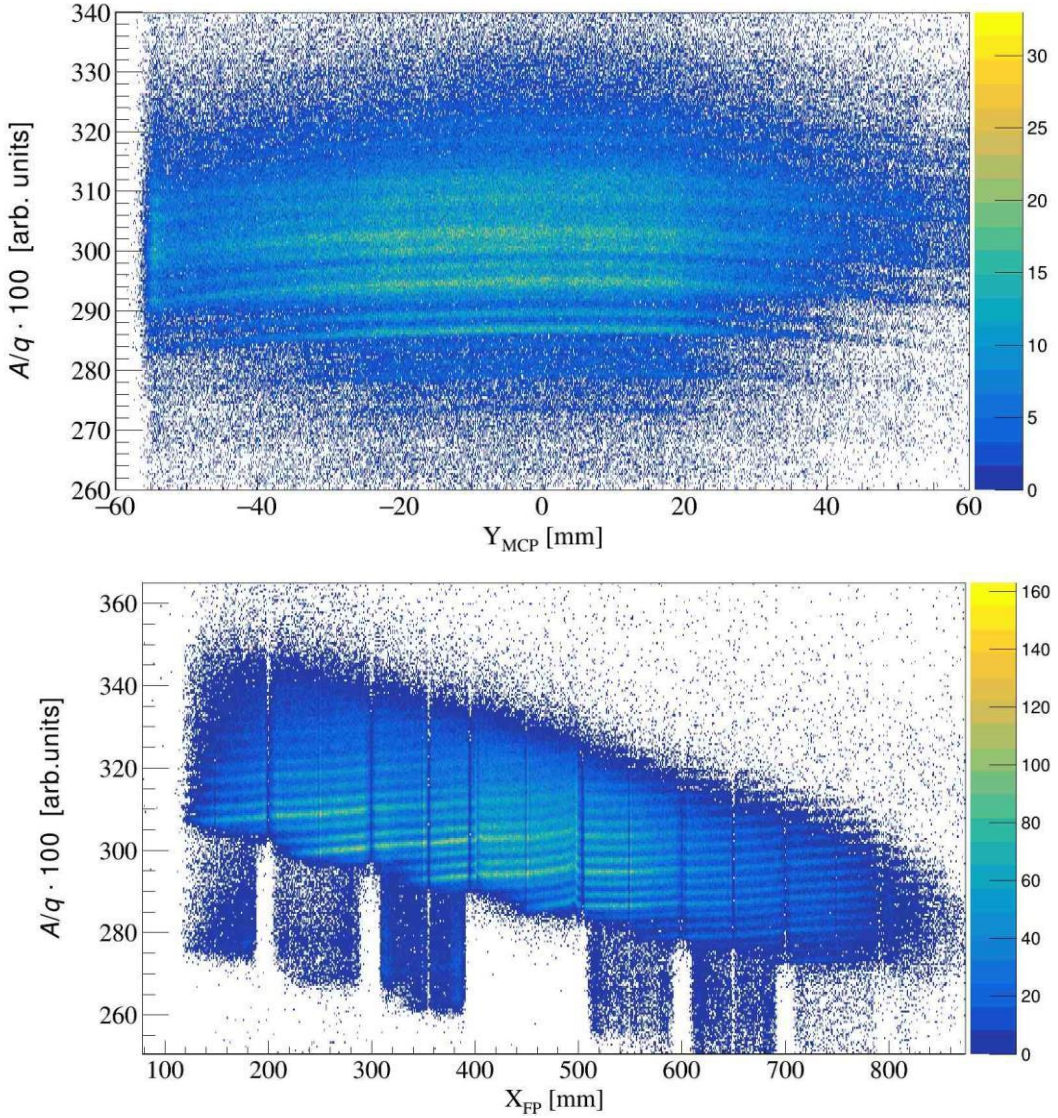

After aberrational corrections

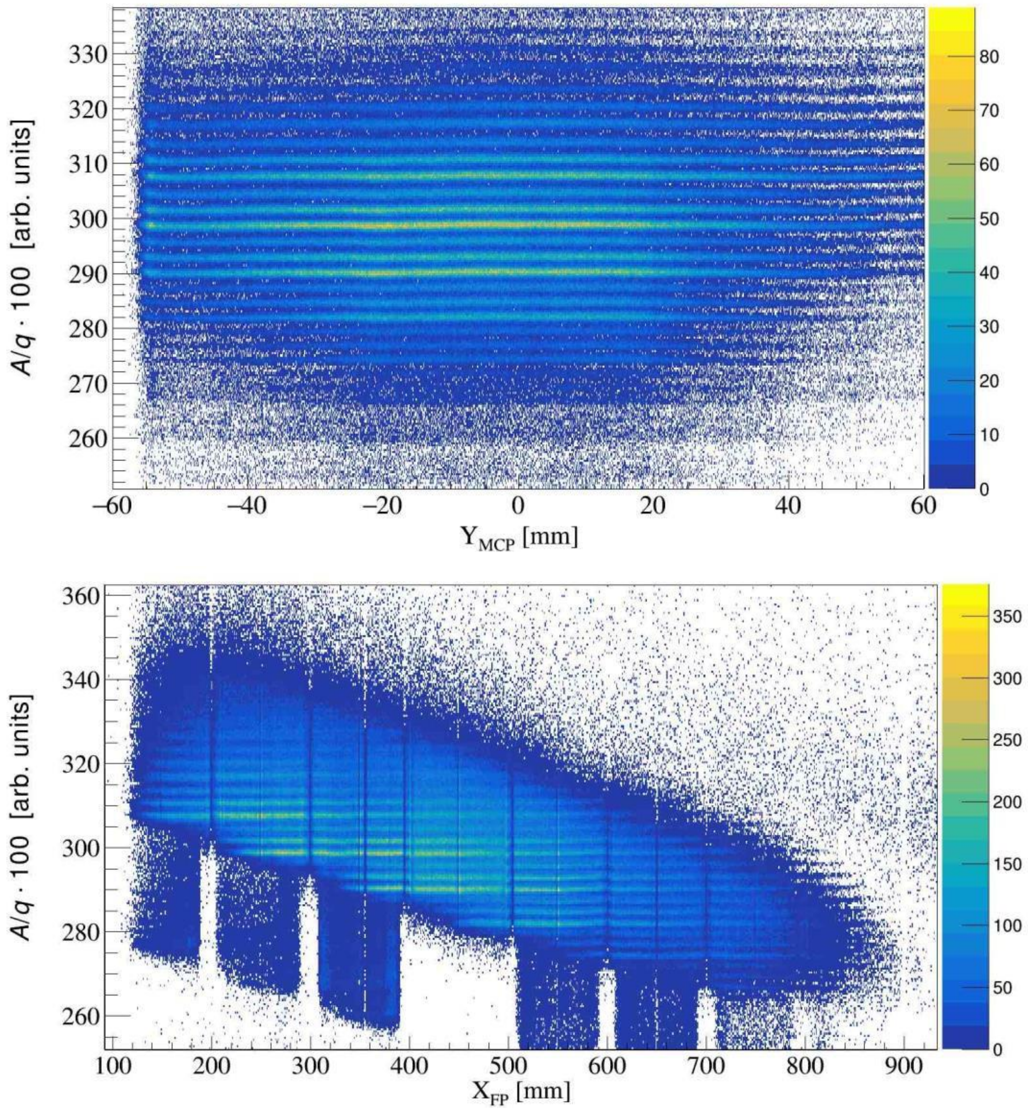

PRISMA - Mass calibration

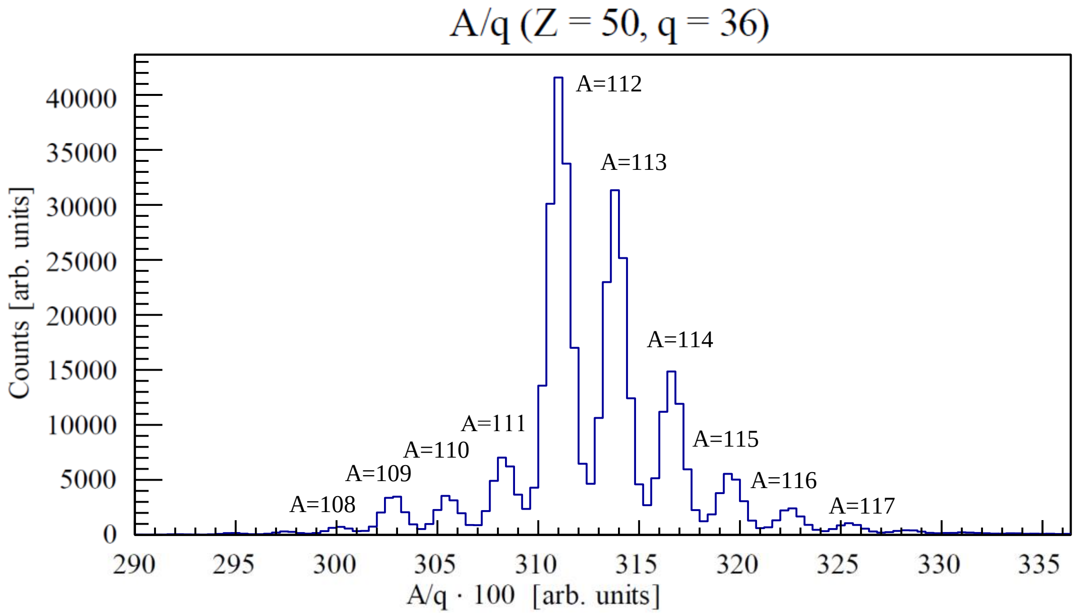

A/q linear calibration applied by measuring centroid of ZQ-gated 1D A/q distributions and comparing observed with expected.

Mass (Z = 50) before linear calibration

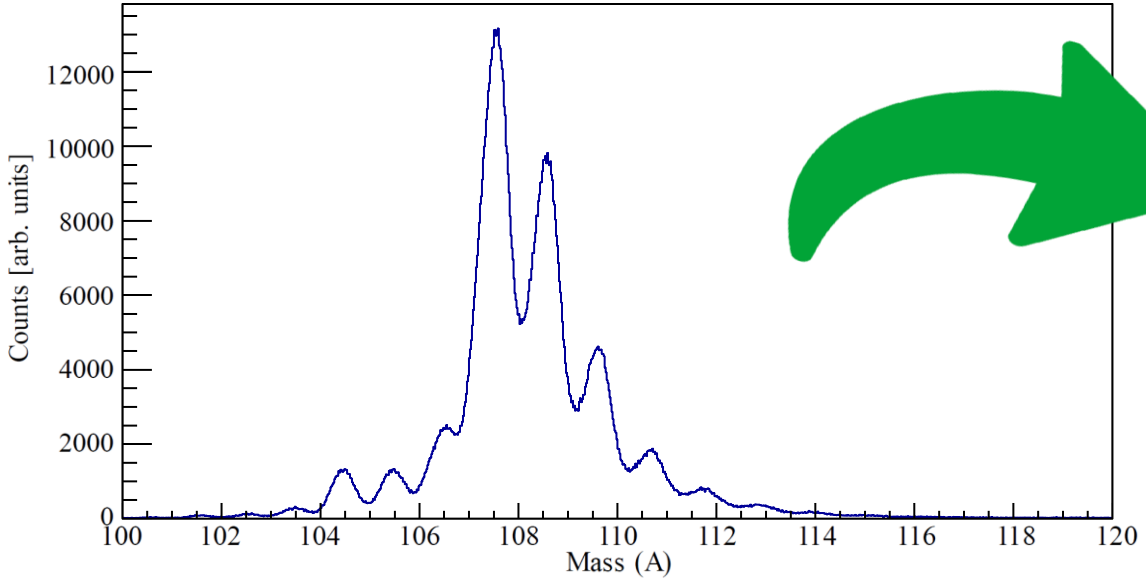

Mass (Z = 50) after linear calibration

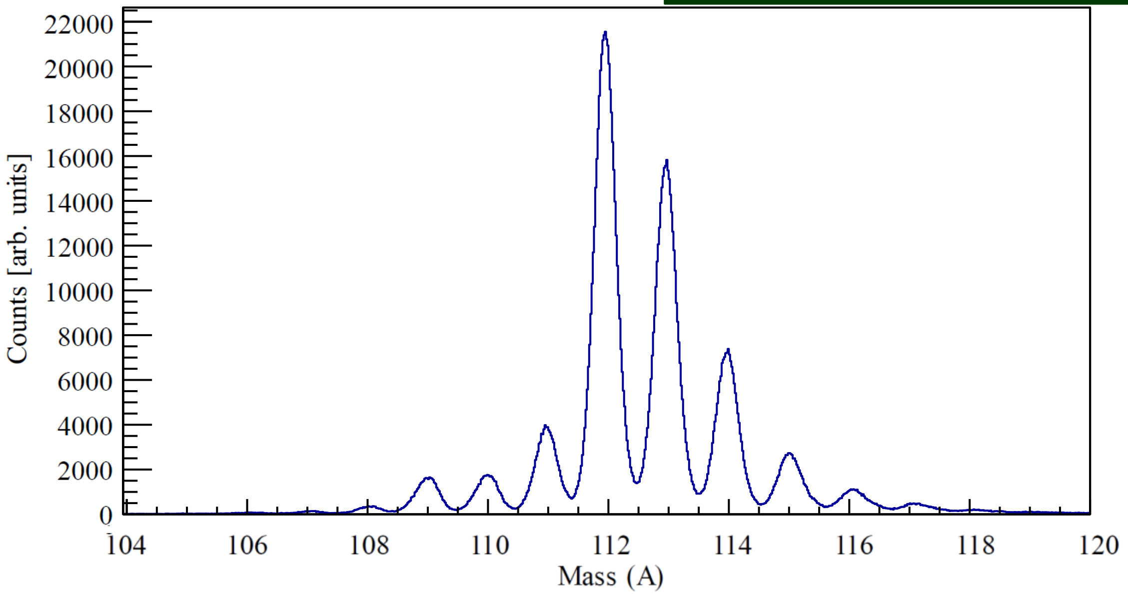

Forward tracking vs. backtracking

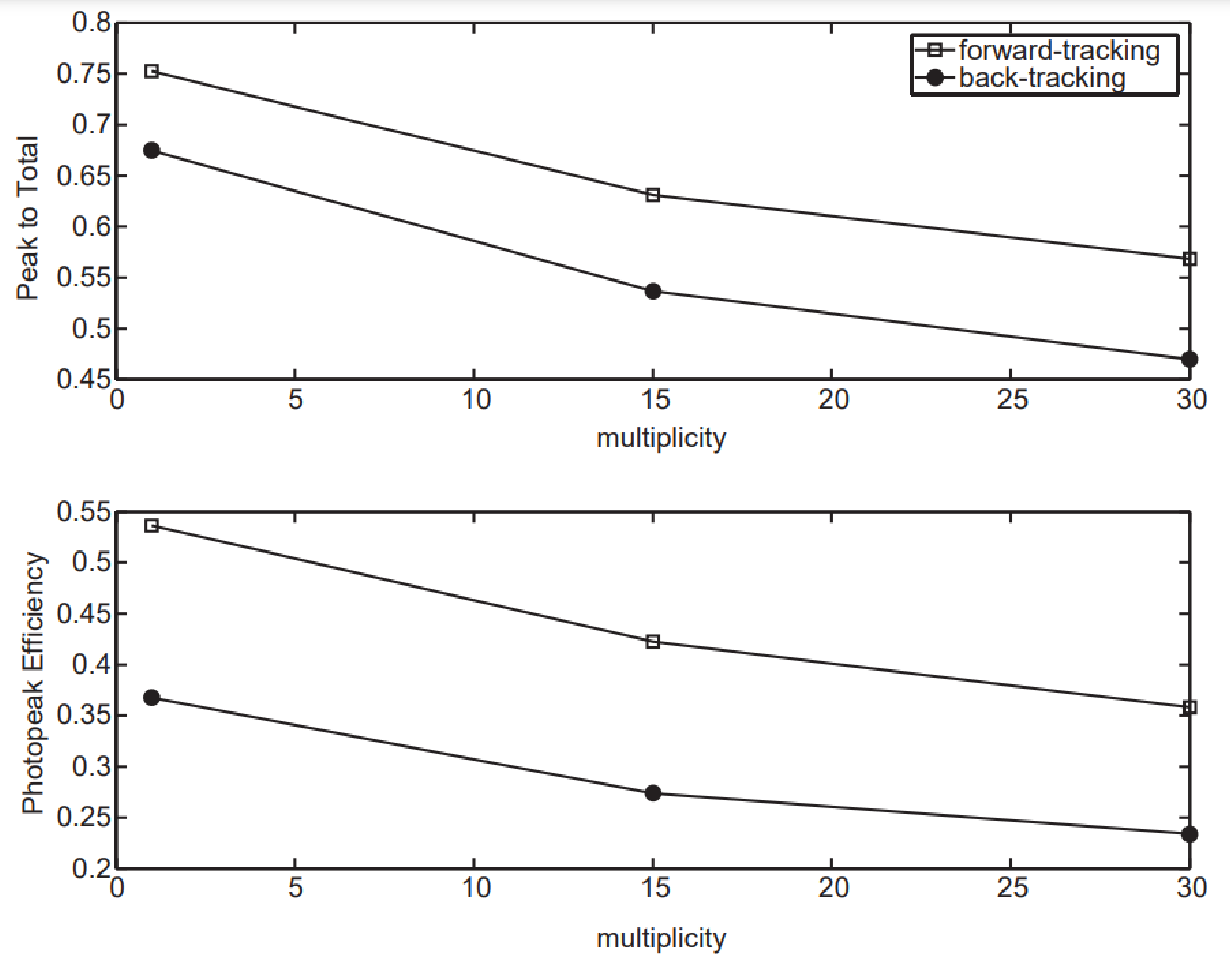

Target ladder

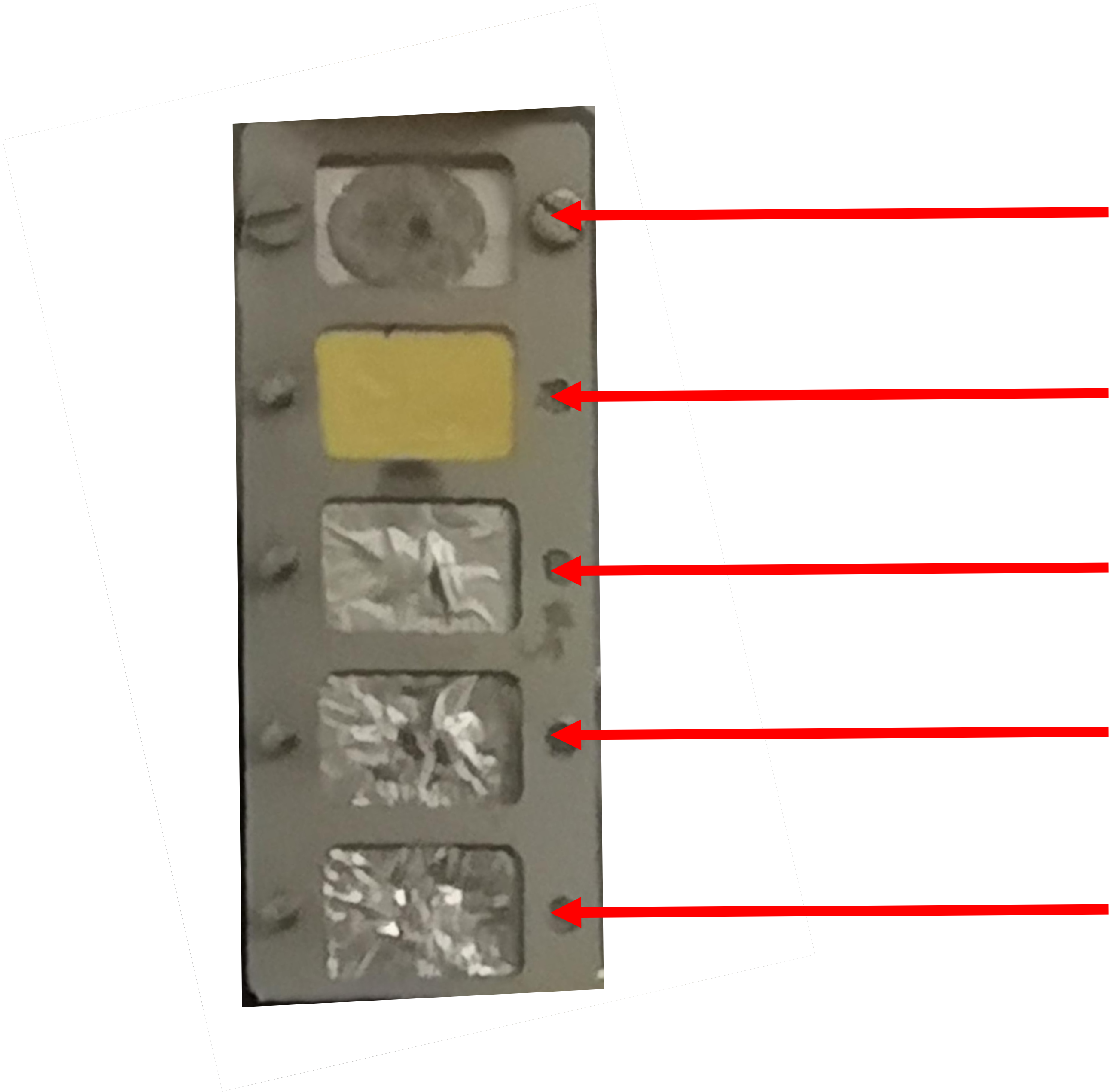

Quartz (beam focusing)

Au (Transmission testing)

^{238}U (1)

^{238}U (2)

^{238}U (3)

Analysis results – AGATA PRISMA coincidences

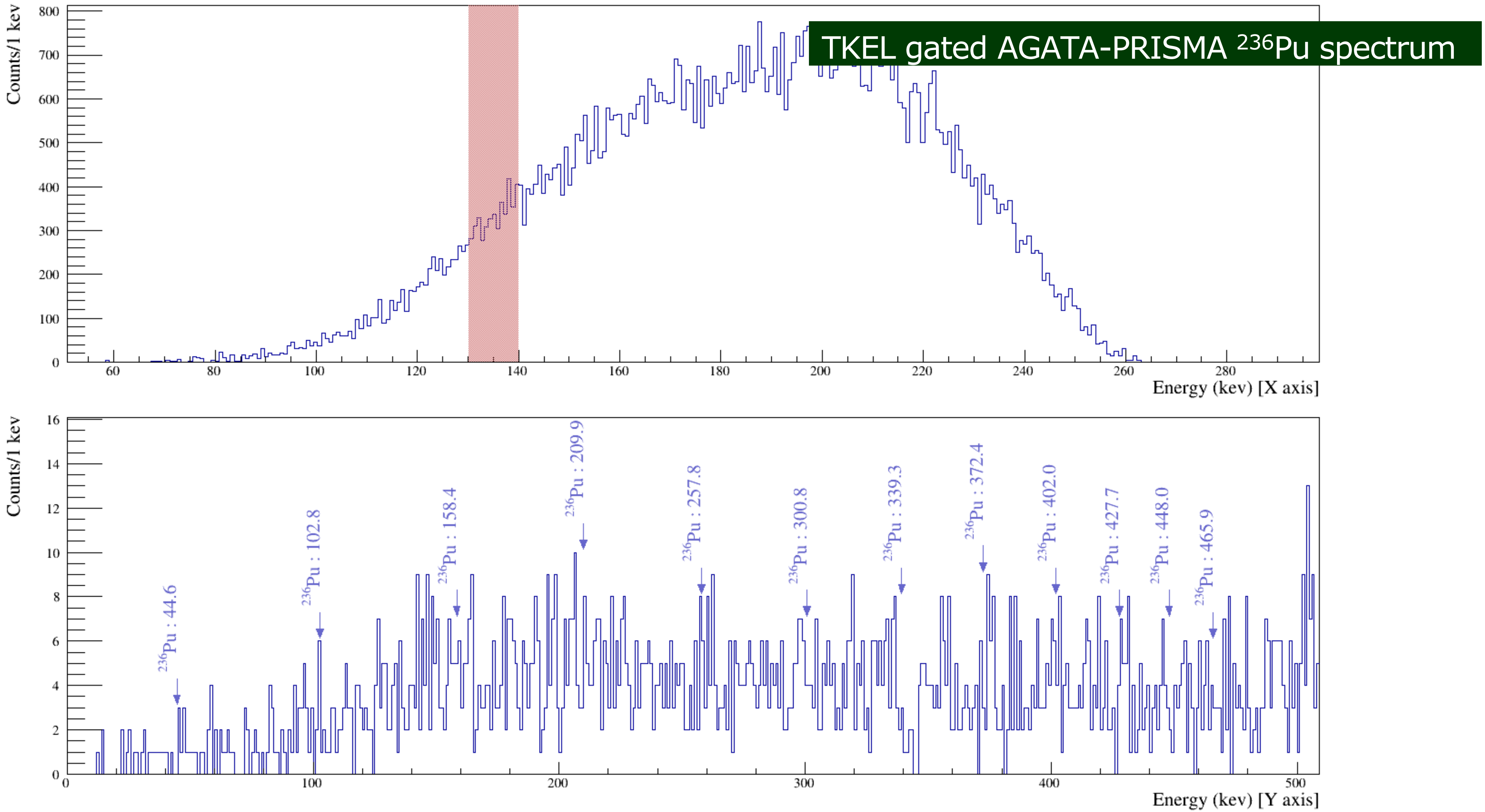

Analysis results – AGATA PRISMA coincidences

AGATA-PRISMA coincidence spectra Analysis ongoing

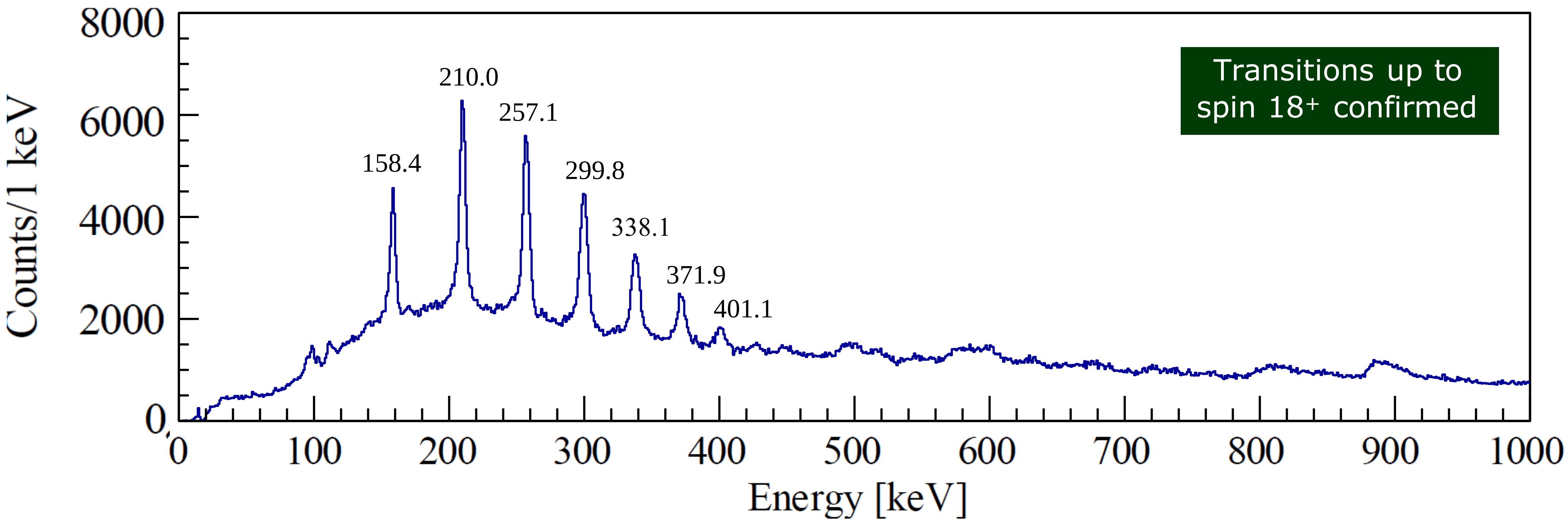

Transitions up to spin 18^+ confirmed

^{238}U Doppler-corrected tracked γ-ray spectra gated on binary partner Sn (Z = 50, A=112).

DANTE Analysis